



**HAL**  
open science

## Crack damage identification of a thick composite sandwich structure based on Gaussian Processes classification

Zeyu Liu, Mohsen Ardabilian, Abdelmalek Zine, Mohamed Ichchou

► **To cite this version:**

Zeyu Liu, Mohsen Ardabilian, Abdelmalek Zine, Mohamed Ichchou. Crack damage identification of a thick composite sandwich structure based on Gaussian Processes classification. *Composite Structures*, 2021, 255, pp.112825. 10.1016/j.compstruct.2020.112825 . hal-03136015

**HAL Id: hal-03136015**

**<https://hal.science/hal-03136015>**

Submitted on 21 Sep 2022

**HAL** is a multi-disciplinary open access archive for the deposit and dissemination of scientific research documents, whether they are published or not. The documents may come from teaching and research institutions in France or abroad, or from public or private research centers.

L'archive ouverte pluridisciplinaire **HAL**, est destinée au dépôt et à la diffusion de documents scientifiques de niveau recherche, publiés ou non, émanant des établissements d'enseignement et de recherche français ou étrangers, des laboratoires publics ou privés.



Distributed under a Creative Commons Attribution - NonCommercial 4.0 International License

# Crack damage identification of a thick composite sandwich structure based on Gaussian Processes classification

Zeyu Liu<sup>a</sup>, Mohsen Ardabilian<sup>b</sup>, Abdelmalek Zine<sup>c</sup>, Mohamed Ichchou<sup>a,\*</sup>

<sup>a</sup>Laboratory of Tribology and Systems Dynamics, École Centrale de Lyon  
36 Av. Guy de Collongue, 69134 Écully Cedex, France

<sup>b</sup>Computer Science Laboratory for Image Processing and Information Systems  
École Centrale de Lyon, 36 Av. Guy de Collongue, 69134 Écully Cedex, France

<sup>c</sup>Institut Camille Jordan, École Centrale de Lyon  
36 Av. Guy de Collongue, 69134 Écully Cedex, France

---

## Abstract

Structural damage of composite materials used in **aeronautics** and aerospace has **attracted increasing attention**. Efficient and reliable Structural Health Monitoring (SHM) systems are required to provide a probabilistic interpretation of diagnostics. In this study, crack damage identification of a thick composite sandwich structure based on Gaussian Processes (GP) classification is reported by numerical simulations. The goal of the study is to obtain a data-driven probabilistic interpretation of damage detection. The investigation is carried out based on healthy and damaged status of a sandwich panel with a honeycomb core modelled in ANSYS. Instantaneous signals with different frequencies are applied to the structure and finite element analysis is performed to obtain vibration responses in both statuses. Features extracted by Discrete Wavelet Transform (DWT) are used to train and test the GP model to assess the health status of the structure. Impacts of mother wavelet in DWT, likelihood function and inference method, as well as iteration numbers are investigated on the classification accuracy. The pertinence of sensors located at different positions is also investigated. This proposed method is effective for crack-type damage detection in the studied composite sandwich structure. It is expected to be suitable for damage detection of more complex structures.

**Keywords:** Structural health monitoring, Gaussian Process classification, composite sandwich structure

---

## 1. Introduction

Advanced composite materials have been widely used in different areas, including aerospace, medicine, machinery, construction and other industries due to the characteristics of light weight, corrosion resistance, heat insulation, sound insulation, shock absorption and high (low) temperature resistance, etc., which typically meet the functional requirements in specific working environments [1]. The application of composite materials is gradually replacing the role of conventional metal alloys in many fields. However, due to the synthesis method of composite materials, they are susceptible to several structural damages, such as fiber fracture, matrix crack and delamination. These damages are usually caused by fatigue and impact events. In the early stage of the damages, they are very small and barely visible to visual inspections, but under certain conditions they may affect the performance of structures and further lead to catastrophic consequences, especially for aircrafts, resulting in huge loss of people lives and money. Therefore, the development of *Structural Health Monitoring (SHM)* systems that can detect damages in a structure has been considerable concerns in the last 2 decades [2].

SHM aims to give, at every moment during the life of a structure, a diagnosis of the "state" of the constituent materials, of different parts, and of the full assembly of these parts constituting the structure as a whole [2]. Health monitoring of structures is initially assessed by visual inspection to approximate the damage location, but damages in bonded structures especially in composite materials are often within the structure and barely visible or even invisible. As a result, several non-destructing testing (NDT) methods that are capable of detecting internally hidden damages are employed during the short inspection intervals [3].

Two of NDT methods, vibration-based technique and guided wave-based technique have been developed for the extraction of damage-sensitive information about the health state of structures. They are the most commonly used among others. A general process of the SHM based on these methods involves collecting relevant data, which is the structure response, from an array of sensors attached on the structure. Then necessary signal processing is carried out for the purpose of data reduction and key feature extraction from these measurements. Finally, the

---

\*Corresponding author

*Email addresses:* zeyu.liu@ec-lyon.fr (Zeyu Liu),  
mohsen.ardabilian@ec-lyon.fr (Mohsen Ardabilian),  
abdel-malek.zine@ec-lyon.fr (Abdelmalek Zine),  
mohamed.ichchou@ec-lyon.fr (Mohamed Ichchou)

32 healthy state of the structure is determined by statistical analysis of these features.  
33 Vibration-based damage detection focuses on the detection of the mode shape  
34 singularity and natural frequency changes created by local discontinuity due to  
35 damages [4–12]. Several researches have successfully implemented this method in  
36 SHM of composite materials. Yang et al. [4] proposed a vibration-based damage  
37 detection method for composite plates with delaminations using modal frequency  
38 surface (MFS). It is found that the effectiveness of the MFS approach depends  
39 on the delamination location by analyzing the modal frequencies. Zhu et al. [5]  
40 proposed a vibration-based NDT to detect debonding in honeycomb sandwich  
41 beams based on the natural frequency changes caused by damages. Honeycomb  
42 sandwich beam is considered equivalent to homogeneous materials in low fre-  
43 quency because the local periodic structure is much smaller than the wavelength.  
44 However, the proposed method cannot effectively detect small damages in large  
45 structures. **A damage indicator based on modal rotational mode shapes obtained  
46 with a uniform rate continuously scanning laser Doppler vibrometer (CSLDV)  
47 technique was proposed by Huang et al. [6] for crack damage detection. The pro-  
48 posed method is proved potential for practical applications, such as ultra-light or  
49 composite structures. It is worth mentioning that in vibration-based NDT, wavelet  
50 analysis has been applied in many studies for the post-processing of vibrational  
51 mode shapes to extract features for damage detection.** Vibration-based NDT with  
52 wavelet analysis was applied to a composite sandwich plate to detect different types  
53 of damages by extracting modal shapes of vibration in the research of Katunin  
54 [7]. Sandwich plate with damages was scanned by **two** laser Doppler vibrometers  
55 (LDV) by experiment and the amplitudes of wavelet analysis coefficients were  
56 used to represent the presence and location of damages. Results show that the  
57 proposed method is capable to detect and localize different damages using wavelet  
58 analysis. But the proposed method should not be limited to the laboratory scale test.  
59 **A novel method for identification of multiple damage by combining shearographic  
60 NDT and 2D undecimated wavelet transform based on modal data was proposed  
61 by Katunin et al. [8]. The proposed method with wavelet analysis shows high  
62 sensitivity compared to the analysis of raw shearographic results. Similar result  
63 was observed in another research conducted by Zhou et al. [9] based on contin-  
64 uous wavelet transform, which shows that the sensitivity for damage detection  
65 is increased by wavelet analysis.** A thorough review of vibration-based damage  
66 detection is presented in [13–15].

67 Guided wave-based damage detection focuses on the detection of discrimi-  
68 native features such as the difference of amplitudes, elastic wave energy variation  
69 and changes in wave propagation pattern due to the interaction between propagated

70 waves and material discontinuity where damage occurs [16–19]. Yu et al. [16] used  
71 ultrasonic feature guided waves (FGW) which focused on the wave propagation  
72 energy to detect damages on quasi-isotropic composite laminates. The interaction  
73 of the identified FGW mode with different types of defects was studied by both  
74 simulation and experiment. Close agreement was observed between the numerical  
75 measurement and experimental measurement. It is demonstrated that the proposed  
76 FGW method has good potential for efficient damage detection in composite bends.  
77 Aryan et al. [17] proposed a model-based method for damage detection with  
78 guided wave. Normally guided wave-based method is conducted by comparing a  
79 baseline signal recorded for a damage-free structure with or subtracted from the  
80 signal recorded during the inspection. In the proposed method, the uncontrollable  
81 factors that may affect the accuracy such as temperature variation, sensor errors  
82 and material property changes due to degradation were compensated. Experimental  
83 and numerical approaches were conducted and demonstrated the feasibility of  
84 the proposed method. Nevertheless, the utilisation of 3D measurement system  
85 together with transient finite element simulations will significantly increase the  
86 cost. Theoretical and numerical studies were conducted by Sikdar et al. to identify  
87 disbond and high density core region in a honeycomb composite sandwich structure  
88 using ultrasonic guided waves [18]. Laboratory experiment was then carried out  
89 to validate theoretical and numerical results. Interaction of guided waves with  
90 damages was analyzed through the structural response signals. A good agreement  
91 was observed between analytical, numerical and experimental results. It is found  
92 that the presence of high density core region results in a decrease in amplitude  
93 of the propagating guided wave modes and the presence of debond results in a  
94 significant amplification of the primary anti-symmetric mode. Similar method  
95 was also adopted in [20–22]. A thorough review of guided wave-based damage  
96 detection methods is presented in [19, 23, 24].

97 To achieve a **better** accuracy in damage detection, Radzienski et al. [25]  
98 combined vibration-based and guided wave-based approaches without reducing the  
99 effectiveness of NDT techniques for detection of debonding in honeycomb core  
100 panels, and higher defect detection reliability was achieved by a double verification.  
101 Both vibration-based and guided wave-based techniques have been proved capable  
102 of detecting damages occurred in composite structures and other materials. They  
103 have good performance in some certain conditions and show a good potential in the  
104 application in more fields. However, a common process of these two methods is that  
105 the vibration responses of a structure should be analysed all by human labor, which  
106 leads to two disadvantages: firstly, they are time-consuming and labor-intensive;  
107 secondly, there will be high requirements of expertise for practitioners during the

108 analysis of structural vibration responses, especially for complex structures, which  
109 is not always available.

110 With the development of Artificial Intelligence (AI) in the last two decades,  
111 the problems encountered in the traditional approaches have been solved. In this  
112 study, a machine learning algorithm Gaussian Process is proposed to predict crack  
113 damages of a thick composite sandwich panel by numerical simulations address-  
114 ing the difficulty in constructing a database for structural health monitoring of  
115 real composite structures and the inconvenience in conventional expertise-based  
116 SHM approaches. The goal of the study is to obtain a data-driven probabilistic  
117 interpretation of damage detection. A squared panel constituted of two composite  
118 faces in carbon/epoxy and a honeycomb core is modelled by commercial software.  
119 The investigation of this structure is carried out based on two status of the model:  
120 healthy model and damaged model. Instantaneous signals with different frequen-  
121 cies are applied to the structure and finite element analysis is performed to obtain  
122 vibration responses in healthy and damaged status, respectively. Features extracted  
123 by discrete Wavelet Transform (DWT) from these responses are fused and defined  
124 as input to the Gaussian Process. The Gaussian Process model is trained and tested  
125 to assess the health status of the structure. The DWT can speed up the computation  
126 time with proper selection of mother wavelet without major loss of information.  
127 The impact of likelihood function and inference methods employed in Gaussian  
128 Process on the classification accuracy is investigated. It is observed that with more  
129 iterations, the classification is slightly better than with less iterations, which is  
130 consistent with common sense. The pertinence of data from sensors located at  
131 different positions is also investigated. Finally, an overall classification accuracy of  
132 100% is obtained, which proves the proposed method is effective for crack-type  
133 damage detection in the studied composite sandwich structure.

134 The rest of this paper is organized as follows: the basic theoretical background  
135 including the feature extraction method DWT as well as machine learning approach  
136 GP will be introduced in section 2. The proposed damage detection system and data  
137 processing technique are explained in section 3. Model description together with  
138 simulation approach are described in section 4, followed by results and discussions  
139 in section 5. Finally, section 6 concludes the paper and suggests potential future  
140 works.

## 141 **2. Theoretical background**

142 The development of data-driven approaches has provided great convenience  
143 in scientific research, but the problem of data redundancy has been an obstacle to

144 efficiency. Ideally, data containing key information are used while useless data are  
145 eliminated. For this purpose, a signal processing and feature extraction method,  
146 Discrete wavelet transform (DWT) is firstly introduced in the current research.  
147 Then conventional machine learning method Gaussian Process will be applied.

### 148 2.1. Feature extraction by Discrete Wavelet Transform

149 DWT was proposed, on one hand, to extract information in both time and  
150 frequency domain **through multi-resolution analysis**, on the other hand to reduce  
151 the dimension of data, which resolves the problem of redundancy. Since the time  
152 domain signal is a discrete time sequence, we denote the sequence as  $x[n]$  with  $n$   
153 an integer. The transform is computed by passing the signal through a half band  
154 digital lowpass filter with impulse response  $h[n]$  and a half band highpass filter  
155 with impulse response  $g[n]$  simultaneously. The filtering, from a mathematical  
156 point of view, is convolution of the signal with the filter. A half band lowpass  
157 filter removes all frequencies above half of the highest frequency in the signal,  
158 whereas a half band highpass filter removes all frequencies below half of the highest  
159 frequency. After passing the signal through filters, detail coefficients from the  
160 output of highpass filter and approximation coefficients from the output of lowpass  
161 filter are obtained. Since half the frequencies of the signal have been removed, half  
162 the samples can be discarded according to Nyquist's theorem. Thus, the output of  
163 lowpass filter is subsampled by 2. This constitutes one decomposition level. This  
164 decomposition has halved the time resolution since the number of samples has  
165 been halved, but has doubled the frequency resolution since the frequency band  
166 has been halved. The subsampled output of lowpass filter is further processed  
167 by passing it again through a new lowpass filter  $h[n]$  and a highpass filter  $g[n]$   
168 constituting another decomposition level. It should be noted that the highpass and  
169 lowpass filters are known as the Quadrature Mirror Filters (QMF) and are related  
170 by:

$$g[L - n - 1] = (-1)^n \times h[n] \quad (1)$$

### 171 2.2. Gaussian Processes classification

172 Supervised machine learning has been widely used to learn a function that  
173 maps an input to an output based on example input-output pairs [26]. As one  
174 sub-field of machine learning, it helps to improve the efficiency and reduce error in  
175 problem solving. It can be divided into regression and classification problems. The  
176 outputs for regression are continuous values whereas for classification are discrete  
177 class labels. The idea of machine learning-based SHM is to learn the relations  
178 between input variables and output variables. One machine learning algorithm that

179 is capable of learning features from data and providing a probabilistic interpretation  
 180 of predictions is Gaussian Process (GP). A GP can be considered as a Gaussian  
 181 distribution over functions rather than over variables, and inference takes place  
 182 directly in the space of functions [27]. A machine learning algorithm involving GP  
 183 takes a measure of the similarity between points to predict the value for an unseen  
 184 point from the training data. There are several GP models for regression problems,  
 185 but in this study, a GP model for classification is employed.

186 An introduction of a GP model for regression problems is firstly carried  
 187 out because it is a necessary step for understanding GP model for classification  
 188 problems. Given an input vector variable  $\mathbf{x}$  with dimension  $D$ , the corresponding  
 189 output target  $t$  is related with the input vector by a nonlinear smooth mapping  
 190 function  $f$  with an additional Gaussian noise  $\epsilon$

$$t = f(\mathbf{x}) + \epsilon \quad (2)$$

191 In the same way, for a given input training data set  $\mathbf{D} = \{\mathbf{X}, \mathbf{t}\}$  containing input  
 192 training matrix  $\mathbf{X} = [\mathbf{x}_1, \mathbf{x}_2, \dots, \mathbf{x}_N]^T$  constituted by vectors  $\mathbf{x}_i$  and corresponding  
 193 training target vector  $\mathbf{t}$ , in which each element is expressed as  $t_i = f(\mathbf{x}_i) + \epsilon$ ,  $i =$   
 194  $1, 2, \dots, N$ , we are interested in making inferences about the relationship between  
 195 inputs and targets as well as making predictions for a new input. Therefore, GP is  
 196 involved by modeling the mapping function  $f$  with a zero mean and covariance  
 197 matrix  $\mathbf{K}$ , see Eq. (3):

$$p(\mathbf{f}|\mathbf{D}) \sim \mathcal{N}(\mathbf{f}|\mathbf{0}, \mathbf{K}) \quad (3)$$

198 where  $\mathbf{f} = [f(\mathbf{x}_1), f(\mathbf{x}_2), \dots, f(\mathbf{x}_N)]^T$ ,  $\mathbf{K}$  is the covariance matrix, computed by  
 199 covariance function  $k(\mathbf{x}_i, \mathbf{x}_j)$ , also called kernel function, expressed by Eq. (4).  
 200 The covariance function is expected to make similar predictions of target values  $t_i$   
 201 and  $t_j$  for similar input points  $\mathbf{x}_i$  and  $\mathbf{x}_j$ . Therefore, the squared exponential with  
 202 automatic relevance determination distance (SE-ARD) measure expressed by Eq.  
 203 (4) is adopted in the present study:

$$k(\mathbf{x}_i, \mathbf{x}_j) = cov(f(\mathbf{x}_i), f(\mathbf{x}_j)) = \sigma_f^2 exp(-\frac{1}{2}(\mathbf{x}_i - \mathbf{x}_j)^T \mathbf{M}(\mathbf{x}_i - \mathbf{x}_j)) \quad (4)$$

204 where  $\mathbf{M} = diag(\lambda_1, \lambda_2, \dots, \lambda_N)$ , with each  $\lambda_i$  corresponding to input dimension  
 205 characteristic length scale.  $\sigma_f^2$  is the signal variance.  $\lambda$  and  $\sigma_f^2$  are hyperparameters.  
 206 In the training step, the objective is to model an appropriate mapping function  
 207  $f$  so that the training target  $t_i$  corresponds well to the training input vector  $\mathbf{x}_i$ .  
 208 The learning task is achieved by tuning the hyperparameters denoted by  $\Theta$  in the  
 209 covariance function. And the optimization is accomplished by minimizing the

210 negative logarithmic likelihood function with respect to the hyperparameters in Eq.  
 211 (5), which corresponds to choosing the value of  $\Theta$  for which the probability of the  
 212 observed data set is maximized.

$$L(\Theta) = -\log(p(\mathbf{t}|\mathbf{X})) = \frac{1}{2} \log |\mathbf{K}| + \frac{1}{2} \mathbf{t}^T \mathbf{K}^{-1} \mathbf{t} + \frac{N}{2} \log(2\pi) \quad (5)$$

213 where  $|\mathbf{K}|$  refers to the determinant of the matrix  $\mathbf{K}$ .

214 The role of the GP model is to use known data  $\mathbf{X}$  and  $\mathbf{t} = [t_1, t_2, \dots, t_N]$  to  
 215 predict the output target of a new input vector  $\mathbf{x}_{N+1}$ . As the covariance matrix  $\mathbf{K}$   
 216 is composed of the covariance between each of the first  $N$  input vectors, for a new  
 217 input vector  $\mathbf{x}_{N+1}$ , the joint probability distribution can be expressed as:

$$p(\mathbf{t}_{N+1}) = \mathcal{N}(\mathbf{t}_{N+1} | \mathbf{0}, \mathbf{K}_{N+1}) \quad (6)$$

218 where  $\mathbf{t}_{N+1} = [t_1, t_2, \dots, t_{N+1}]^T$ , and the covariance matrix  $\mathbf{K}_{N+1}$  is expressed as:

$$\mathbf{K}_{N+1} = \begin{bmatrix} \mathbf{K} + \sigma_n^2 \mathbf{I} & \mathbf{k} \\ \mathbf{k}^T & c \end{bmatrix} \quad (7)$$

219 with  $\mathbf{k}$  a vector with elements  $k(\mathbf{x}_n, \mathbf{x}_{N+1})$  for  $n = 1, 2, \dots, N$ , and  $c$  a scalar with  
 220 value  $c = k(\mathbf{x}_{N+1}, \mathbf{x}_{N+1}) + \sigma_n^2$ . It's clear to see that the vector  $\mathbf{k}$  and the scalar  $c$   
 221 are both dependant on the test point input vector  $\mathbf{x}_{N+1}$ . The predictive conditional  
 222 distribution over  $t_{N+1}$  is a Gaussian distribution with mean and covariance given  
 223 by [28]:

$$\begin{aligned} \mu(\mathbf{x}_{N+1}) &= \mathbf{k}^T \mathbf{K} \mathbf{t}, \\ \sigma^2(\mathbf{x}_{N+1}) &= c - \mathbf{k}^T \mathbf{K} \mathbf{k} \end{aligned} \quad (8)$$

224 These two items are the most important for the regression because they provide both  
 225 prediction mean value and uncertainty information. In a GP regression example,  
 226 the regression problem is resolved by making a prediction of a new target for a  
 227 new input with a predictive mean value and uncertainty information indicated by a  
 228 confidential interval. It shows the more sparse the data, the larger the uncertainty  
 229 interval of the prediction.

230 For a classification problem, our goal is to model the posterior probability  
 231 distribution of the target for a new input vector, given a set of training data. The  
 232 predictive probabilities should be in the interval  $[0, 1]$ , but the prediction result of  
 233 the Gaussian Process is within the entire real range. However, GP model can be  
 234 adapted to classification problems by transforming the output using an appropriate  
 235 nonlinear activation function, such as logistic sigmoid:

$$\sigma(f) = \frac{1}{1 + \exp(-f)} \quad (9)$$

236 Consider a binary classification problem with target value  $t \in \{-1, 1\}$ . A  
 237 Gaussian Process is defined over a function  $f(x)$  and then this function is trans-  
 238 formed by a logistic sigmoid  $y = \sigma(f)$ , with  $y \in (0, 1)$ . The probability distribu-  
 239 tion of the target variable is given by the Bernoulli distribution:

$$p(t|f) = \sigma(f)^t(1 - \sigma(f))^{1-t} \quad (10)$$

240 Similar to the regression, the training input vectors are denoted by  $\mathbf{x}_1, \mathbf{x}_2, \dots, \mathbf{x}_N$ ,  
 241 the corresponding observed targets are denoted by  $\mathbf{t}_N = [t_1, t_2, \dots, t_N]^T$ . The  
 242 objective is to determine the predictive distribution of  $p(t_{N+1}|\mathbf{t}_N)$ . In classification  
 243 problems, the Gaussian noise  $\epsilon$  in covariance matrix no longer exists because  
 244 it is assumed that every training input vector is correctly labelled. In a two-  
 245 class problem, predicting  $p(t_{N+1} = 1|\mathbf{t})$  is enough because the probability of  
 246  $p(t_{N+1} = -1|\mathbf{t})$  is obtained by  $1 - p(t_{N+1} = 1|\mathbf{t})$ . The expected predictive  
 247 distribution is obtained by a marginal distribution expressed as:

$$p(t_{N+1} = 1|\mathbf{t}) = \int p(t_{N+1} = 1|f_{N+1})p(f_{N+1}|\mathbf{t})df_{N+1} \quad (11)$$

248 where  $f_{N+1} = f(\mathbf{x}_{N+1})$ . However, this integral is analytically intractable. To  
 249 approximate the integral, several inference methods can be taken into account, such  
 250 as Laplace approximation, variational inference, expectation propagation, etc.

### 251 **3. Proposed Gaussian Processes classification method for composite sand-** 252 **wich structure**

253 The proposed Gaussian Process includes 2 main steps: training step and  
 254 testing step for the purpose of classification using the processed signals from  
 255 sensors. In the first step, training for each case corresponding to healthy and  
 256 damaged structural status is performed. The training data is correctly labeled. In  
 257 the second step, the GP model obtained from previous step is used to evaluate  
 258 unknown features so as to determine if damages appear in the structure or not.

#### 259 *3.1. Training step*

260 Damage detection of a structure is achieved by a SHM system consisting of  
 261 several sensors permanently attached on the structure. Each sensor can be used  
 262 as an actuator to apply an pulse excitation signal or as a receiver to collect data.  
 263 In each simulation scenario, a pre-defined pulse signal is applied on the actuator.  
 264 The signal interacts with elements of the structure during the propagation over

265 the whole structure. Sensors located at three corners are considered capable of  
 266 collecting signals that have interacted with potential damages without missing  
 267 information. These raw time series signals are processed with Discrete Wavelet  
 268 Transform. This step can be regarded as reduction of data dimension and feature  
 269 extraction because DWT is used to extract information in both time and frequency  
 270 domains as well as discarding data that is not dominant without any major loss of  
 271 information. The Coiflet 5 is chosen as mother wavelet after comparing with other  
 272 wavelets. This wavelet is the optimal among others in terms of errors.

273 In each simulation case, one file containing signals collected by three sensors  
 274 is obtained. It should be noted that, the duration of each simulation is 0.01s and  
 275 the sampling frequency depends on the input signal frequency, thus the number  
 276 of sampling points for a fixed time duration is different for different signals. Note  
 277 that in DWT the successive subsampling is by 2, the collected signal length should  
 278 be a power of 2 or a multiple of power of 2 in order to make the scheme efficient.  
 279 Thus, the first 512 sampled points for signals whose length is more than 512 are  
 280 used for DWT, while for collected signals whose length is less than 512, zeros  
 281 are added after each signal until its length becomes 512. DWT is employed for  
 282 each collected signal, and the corresponding coefficients are saved as one vector.  
 283 Since the frequency bands that are not very prominent in the original signal will  
 284 have very low amplitudes, that part of the DWT signal can be discarded without  
 285 any major loss of information. For this reason, only the first 256 coefficients are  
 286 used, as shown in figure 1. In each simulation, the three vectors after reduction  
 287 obtained by DWT are merged into one vector which contains all features from  
 288 different sensors in the order of the sensors. The same procedure is performed for  
 289 all simulation cases. All the vectors are organized in one matrix in which each row  
 290 consists of one transposed vector representing one simulation. This matrix contains  
 291 all features of the structures and this procedure is considered as data fusion.

292 The matrix after data fusion is in the form of:

$$\mathbf{X} = \begin{pmatrix} x_{11}^1 & \cdots & x_{1K}^1 & x_{11}^2 & \cdots & x_{1K}^2 & \cdots & x_{11}^J & \cdots & x_{1K}^J \\ \vdots & \ddots & \vdots & \vdots & \ddots & \vdots & \cdots & \vdots & \ddots & \vdots \\ x_{I1}^1 & \cdots & x_{IK}^1 & x_{I1}^2 & \cdots & x_{IK}^2 & \cdots & x_{I1}^J & \cdots & x_{IK}^J \end{pmatrix} \quad (12)$$

293 where the element is denoted by  $x_{ik}^j$  in which  $i$  indicates the simulation number  
 294 ( $i^{th}$  simulation),  $j$  indicates the sensor number ( $j^{th}$  sensor) and  $k$  indicates the  
 295 coefficient number ( $k^{th}$  coefficient). Group scaling is performed on this matrix in  
 296 order to remove the mean trajectories of each sensor and to make sure that data  
 297 from any sensor have the same variance [29]. The element in the matrix is scaled

298 by:

$$\bar{x}_{ik}^j = \frac{x_{ik}^j - \mu_k^j}{\sigma^j} \quad (13)$$

299 where  $\mu_k^j = \frac{1}{I} \sum_{i=1}^I x_{ik}^j$  is the mean of the  $I$  measurements of sensor  $j$  for the

300  $k^{th}$  coefficient,  $\sigma^j = \sqrt{\frac{1}{IK} \sum_{i=1}^I \sum_{k=1}^K (x_{ik}^j - \mu^j)^2}$  is the standard deviation of all

301 measurements of sensor  $j$ , and  $\mu^j$  is the mean of all measurements of sensor  $j$ .  
302 This scaled matrix  $\bar{\mathbf{X}}$  is used as input of Gaussian Process for subsequence analysis.

303 In GP training step, input vectors in the matrix  $\bar{\mathbf{X}}$  are correctly labelled by the  
304 ground truth  $t$  with  $t = 1$  indicating *healthy status* and  $t = -1$  indicating *damaged*  
305 *status*. Likelihood function together with inference method are employed. These  
306 two functions are specified in the training step. Hyperparameters are predefined  
307 randomly for the purpose of initialization. The input is then fed into the GP model  
308 and in turn an output predicted by the model is given. During the learning process,  
309 negative logarithmic likelihood function is used as loss function to optimize all  
310 hyperparameters in kernel function and likelihood function so that the error between  
311 the predictive output derived from GP and the corresponding ground truth is  
312 minimized. The optimization process is achieved by minimizing the negative  
313 logarithmic likelihood function with respect to the hyperparameters  $\Theta$ , which  
314 corresponds to choosing the value of  $\Theta$  for which the probability of the observed  
315 data set is maximized. This procedure is illustrated in figure 2.

### 316 3.2. Testing step

317 Once the hyperparameters are optimized for the training data, the validated  
318 GP model can be used to make predictions for new inputs. In this study, the GP  
319 model is used to predict if damages occur in the structure. The testing procedure  
320 is the same as that of training before inserting the transformed input into the GP  
321 model. In testing step, only the trained GP model is used. Besides, different from  
322 the training phase where optimized hyperparameters are as output, the trained GP  
323 model will provide a predictive mean value corresponding to the new input and a  
324 variance of the predictive distribution based on the training data. The predictive  
325 mean value indicates in which label class the input is most likely distributed, that's  
326 to say healthy or damaged class, while the variance provides an information of  
327 confidence, which indicates the reliability of the classification result. It should be  
328 noted that the GP model is used to predict the appearance of damages, but unable

329 to localized the probable region where damages occur. The procedure of the testing  
330 step is presented in figure 3.

#### 331 **4. Numerical approach**

332 In data driven-based SHM systems, information containing the structure's  
333 health status is quite important for the performance of the system. Thus, perti-  
334 nent structural status should be collected to construct a reliable database because  
335 different sets of data correspond to different healthy conditions of a structure.  
336 However, it is neither economic nor realistic to build real structures of different  
337 health status, especially for huge and expensive structures to construct a database.  
338 To understand the behaviour of a structure, numerical simulation of structures in  
339 different conditions is a promising idea. Therefore, SHM achieved by simulation  
340 becomes a compromise way. This study is conducted by simulation approach.  
341 The structure is constructed with software ANSYS® and numerical model under  
342 external excitation is simulated within the software.

##### 343 *4.1. Composite sandwich plate model*

344 In the present work, a hexagonal shaped Nomex honeycomb core (3D core)  
345 and CFRP-skin made composite sandwich plate is selected for simulation and  
346 classification tasks. The plate of spatial dimensions  $300\text{ mm} \times 294\text{ mm} \times 19$   
347  $\text{mm}$  consists of a honeycomb core and two face sheets. The thickness of the  
348 honeycomb core is  $H = 15\text{mm}$  in which the radius and wall thickness of each cell  
349 are  $r = 5\text{mm}$  and  $t = 0.2\text{mm}$ , respectively. The Nomex core's material properties  
350 are: density  $\rho_1 = 1240\text{kg/m}^3$ , Poisson's ratio  $\nu_1 = 0.33$ , Young's modulus  
351  $E_1 = 5.5 \times 10^9\text{Pa}$ . The thickness of each face sheet is  $h = 2\text{mm}$ . The face sheets  
352 are laminate panels made of carbon/epoxy materials whose properties are: density  
353  $\rho_2 = 1850\text{kg/m}^3$ , Poisson's ratio  $\nu_2 = 0.3$ , Young's modulus  $E_2 = 70 \times 10^9\text{Pa}$ .  
354 A simplifies illustration of the sandwich structure is referred to figure 4(a).

355 The honeycomb sandwich plate model consisting of a honeycomb core and  
356 two skin plates is shown in figure 4(b). Within our study the dimensions of the  
357 face sheets and the core will not change.

358 The face sheets are modeled by the SOLSH190 solid-shell element which  
359 has 8 nodes with 3 degrees of freedom at each node: translation in x, y and z  
360 directions. In this manner, face sheet shear phenomena can be taken into account  
361 when a signal with high frequency propagates in the structure. 2D shell element  
362 SHELL181 is used to model the honeycomb cells. The transition area where the  
363 face sheet connect to the honeycomb cell is often the weakest region. In our study,

364 the elements of shell and solid-shell are connected with an automatic constrain  
365 equation developed by ANSYS<sup>®</sup>. The total number of meshing elements is about  
366 177000, which guarantees a minimum mesh density of 10 elements per wavelength  
367 for the model.

368 Composite materials exposed to long term loads and critical working environ-  
369 ment may have damages due to fatigue, impact or material degradation. Cracks and  
370 delamination are two most common damages for composites. In the first attempt  
371 of this study, crack damage is designed in the sandwich structure by disconnecting  
372 local nodes and investigation of the capability of detecting this kind of damage is  
373 conducted. Models with cracks in different positions are constructed. Five crack  
374 damages in the x direction and one crack damage in y direction are created. Cracks  
375 in x direction are located at  $(x = \frac{L}{4}, y = \frac{W}{4})$ ,  $(x = \frac{L}{4}, y = \frac{W}{2})$ ,  $(x = \frac{L}{2}, y = \frac{W}{4})$ ,  
376  $(x = \frac{L}{2}, y = \frac{W}{2})$ ,  $(x = \frac{3L}{4}, y = \frac{3W}{4})$ , respectively. Crack in y direction is located  
377 at  $(x = \frac{L}{2}, y = \frac{W}{2})$ . The length of cracks is 30mm which is  $\frac{L}{10}$  in x direction, and  
378 crack length in y direction is 43mm, as illustrated in figure 5. Cracks are designed  
379 through the core and the top face sheet so that the interaction of the propagated  
380 signal with the damage is detectable.

381 For each model, points located in four corners on the top face sheet are  
382 selected. One is used as actuator through which the pulse excitation signal is  
383 inserted, while the other three are used to collect propagated signals through the  
384 structure, as shown in figure 5(a). In actual cases, the actuator converts the input  
385 voltage signal into a displacement signal, whereas the sensor converts the received  
386 displacement signal into a voltage signal. Thus in the current study, for the sake of  
387 convenience, we directly input the displacement signal on the structure and extract  
388 the displacement signal at the corresponding position to represent the work of  
389 actuator and sensors. The vertical displacement of nodes are collected for further  
390 signal processing.

#### 391 4.2. Simulation

392 In the simulation of each model, a pulse excitation signal with 7 cycles is  
393 applied on the actuator to stimulate vertical displacement. Transient analysis  
394 is performed on the sandwich plate structure. Damping coefficients are set as  
395 follows: matrix multiplier is set as  $\alpha = 0$  and stiffness matrix multiplier as  
396  $\beta = 6.37 \times 10^{-7}$ . The calculation time is set as 0.01s, which is long enough  
397 for the wave to propagate through the whole plate. The sampling frequency  $f_s$   
398 should be no less than 2 times the signal frequency  $f$  according to the Nyquist's  
399 rule. In the present research the sampling frequency is set as  $f_s = 8f$  in order  
400 to make the recorded signal be representative. In each simulation case, vibration

401 responses of one structure are collected at three sensors for further use. They are  
402 saved in one file to represent the structural health status in that condition. Same  
403 simulations are performed for the same structure with input signals of different  
404 frequencies. Then the same simulations are conducted for structures with different  
405 health status successively. As mentioned above, we have 7 composite sandwich  
406 plate models among which one healthy and six with crack damages at different  
407 positions. On each model 3 different input signals with frequency 8kHz, 6kHz and  
408 4kHz are applied successively corresponding to 3 simulation cases. So far a total  
409 of 21 simulation cases are obtained. The objective is to perform the least cases  
410 with which machine learning approaches can detect the structure's health status.

411 A comparison of the vibration responses of a healthy structure and the structure  
412 in figure 5(b) to a same input signal of 8kHz with 7 cycles at the same position  
413 is firstly conducted, as shown in figure 6. The compared signals are from three  
414 sensors on the structure together with the input signal. First of all, in both structures  
415 it can be seen that the original input excitation signal waveform has changed after  
416 propagating along different directions by comparing the signals in figure 6(b-d)  
417 with figure 6(a). This is due to the wave dispersion in the structure. Besides, as the  
418 core of the structure is honeycomb that has anisotropic properties, the dispersive  
419 behavior of the structure is direction-dependant, which results in the differences  
420 in the vibration responses from 3 sensors in figure 6(b) to figure 6(d). Moreover,  
421 comparing the vibration responses of healthy and damaged structures from sensor  
422 3, we can find that in the first wave packet, the amplitude of the signal from  
423 damaged structure is slightly higher than that from healthy structure, as shown in  
424 6(d). It is due to the fact that the existence of the crack damage in this position  
425 reduces the bending stiffness of the structure in y direction from the actuator to  
426 sensor 3. Furthermore, comparing the healthy and damaged structures in 6(b)  
427 and (d), the signal difference occurring between wave packets might be caused by  
428 the interaction of input signal with the crack, but as the difference is not evident,  
429 machine learning algorithm should be used to learn such kind of features.

430 The DWT coefficients are then compared in figure 7. As mentioned in 2.1,  
431 DWT can extract information in both time and frequency domain. The mismatch  
432 between the vibration responses of healthy and damaged structures can be extracted,  
433 as shown in figure 7(b) and (d). It should be noted that only the first 256 coefficients,  
434 which correspond to lower frequencies of the analysis, carry relevant information  
435 and the rest of the signal can be discarded without any major loss of information.  
436 In addition, discarding half of the signal can speed up the computation in further  
437 step.

438 For the six sandwich models with cracks, simulations are conducted with

439 excitation signals of three different frequencies successively. 30 data sets for each  
440 model are collected. For the damage-free sandwich model, same simulations are  
441 conducted with excitation signals of three different frequencies successively as for  
442 the damage models. 90 data sets are obtained. Thus a data base is constructed with  
443 a total number of 270 data sets, in which 90 data for healthy model which is labeled  
444 by '1' and 180 data for damaged models labeled by '-1'. 70% of the data base is  
445 used for training the GP model and the rest 30% is used for testing. The testing step  
446 is a step for evaluating the GP model for damage predictions in composite sandwich  
447 plates. In both training and testing step, several factors will affect the results, such  
448 as the type of mother wavelet for the DWT, the amount of data discarded by DWT,  
449 the selection of likelihood function and inference method for GP, and the number  
450 of function evaluations to optimize hyperparameters during the training step, etc.  
451 The influence of these factors will be evaluated successively. It is worth mentioning  
452 that although discarding the coefficients that have low amplitude in DWT may not  
453 lead to major loss of information, **it will slightly reduce the accuracy of the results,**  
454 **but the effect is negligible.**

## 455 **5. Results and discussions**

456 In this section, the influence of previously mentioned factors on the classifica-  
457 tion results is discussed. In binary classification case, 1 represents healthy status  
458 while -1 represents damaged status. It is expected that the predictive mean value  
459 is as close to 1 as possible for the case whose ground truth is healthy, while the  
460 predictive mean value is as close to -1 as possible for the case whose ground truth  
461 is damaged. However, in GP classification model, the predictive mean value is not  
462 necessarily 1 or -1. Therefore, it is necessary to define a threshold to determine if  
463 the prediction from the GP model is correct or not. In the testing step, an overall  
464 predictive mean value for each class can be calculated,  $\mu_d$  for damaged class and  
465  $\mu_h$  for healthy class. The threshold to separate two classes is defined as the mean  
466 value of  $\mu_d$  and  $\mu_h$ . The distance from overall mean value to the threshold is called  
467 class distance, which is considered as a measure of the quality of the classifier. If  
468 the predictive mean value for a case whose ground truth is damaged is less than  
469 the threshold, the prediction is considered as correct, indicating a damaged status.  
470 The same, if the predictive mean value for a case whose ground truth is healthy is  
471 greater than the threshold, then it means that the status of the structure is predicted  
472 as healthy by GP model, which is correct. Otherwise, it is considered that the GP  
473 model misclassifies the case.

474 *5.1. Classification with three sensors*

475 Firstly, the influence of the selection of mother wavelet is investigated. Control  
 476 variate method is employed, that's to say in each analysis, only one factor is  
 477 considered as a variable while others are invariant. Daubechies 8 (D8) wavelet and  
 478 Coiflet 5 (C5) wavelet are compared with 512 saved coefficients in DWT, logistic  
 479 function as likelihood function, Variational Bayesian (VB) as inference method.  
 480 40 iterations are adopted in the optimization step, see figure 8. The abbreviation  
 481 of mother wavelet, saved amount of data in DWT, likelihood function, inference  
 482 method and iteration numbers are successively listed in the legend on the up-left of  
 483 the figure. It should be noted that in all the following figures, the first 54 testing  
 484 points (denoted by  $\square$ ) along the x-axis are with ground truth 'Damage' while the  
 485 last 27 testing points (denoted by  $*$ ) are with ground truth 'Health'. The global  
 486 mean value of predictive mean value for all testing damaged cases and that for  
 487 healthy cases are  $-0.885$  and  $0.775$  using Coiflet 5 wavelet, while the results using  
 488 Daubechies 8 wavelet are  $-0.858$  and  $0.697$  respectively. In addition, every single  
 489 case is correctly classified using Coiflet 5 wavelet, which suggests that Coiflet 5 is  
 490 more powerful in extracting features. It should be noted that some other mother  
 491 wavelets are also evaluated but have poorer performance and **the corresponding**  
 492 **results are listed in Table 1. the class distance is larger than others while the mean**  
 493 **square error is lower, which indicates that** the GP model performs better in the  
 classification for both healthy and damaged structures using Coiflet 5 wavelet.

	Haar	Beylkin	Coiflet5	Coiflet3	Coiflet1
Class distance	0.5261	0.8344	0.8803	0.8161	0.8697
MSE	0.0799	0.0374	0.0087	0.0214	0.0135
	D20	D16	D12	D8	D4
Class distance	0.8397	0.8380	0.8408	0.8363	0.8268
MSE	0.0172	0.0140	0.0133	0.0354	0.0251
	Symlet10	Symlet8	Symlet6	Symlet4	Vaidyanathan
Class distance	0.8738	0.8323	0.8575	0.8578	0.8320
MSE	0.0145	0.0329	0.0121	0.0172	0.0162

Table 1: Performance of different wavelets in GP classification.

494 Secondly, the influence of the amount of data discarded by DWT on the  
 495 classification accuracy is discussed. According to the previous study, Coiflet  
 496 5 mother wavelet, Logistic likelihood function, Variational Bayesian inference  
 497 method and 40 iterations are used due to the outstanding performance. An example  
 498

499 of DWT coefficients is illustrated in figure 1. All 512 coefficients and the first  
500 256 coefficients are separately used for GP model to study the influence on the  
501 classification accuracy. Results without discarding coefficients is slightly better  
502 than those discarding the last 256 coefficients that have low amplitude, as shown in  
503 figure 9, which is reasonable and easy to understand, because although discarding  
504 the coefficients that have low amplitude in DWT may not lead to major loss of  
505 information, **it will slightly reduce the accuracy of the results, but the effect is**  
506 **negligible.**

507 Thirdly, the influence of likelihood function and inference method is investi-  
508 gated simultaneously because there is an issue of compatibility among different  
509 likelihood functions and inference methods. Four combinations of likelihood  
510 function and inference method are presented in figure 10, including Logistic-VB,  
511 Logistic-Expectation Propagation (EP), Logistic-Laplace and Error function (Erf)-  
512 EP. It can be seen that the Logistic-Laplace combination performs the worst because  
513 the predictive mean value for almost all cases are around 0 and far from 1 or -1,  
514 which shows that the class distance is too short. The global predictive mean value  
515 for healthy and damaged cases are 0.281 and  $-0.22$  respectively. The Logistic-EP  
516 combination and Erf-EP combination perform better than Logistic-Laplace, with  
517 a global mean value  $\mu_h = 0.714, \mu_d = -0.546$  and  $\mu_h = 0.745, \mu_d = -0.622$ ,  
518 respectively. However, 3 cases are misclassified with Logistic-EP combination and  
519 3 cases are misclassified with Erf-EP combination. A better result is achieved by  
520 Logistic-VB combination with global mean value  $\mu_h = 0.667, \mu_d = -0.891$  where  
521 the class distance is larger than others, indicating a better classification quality, and  
522 only 1 case is misclassified.

523 Finally, the influence of iteration numbers on the accuracy of the classification  
524 results is discussed. The iteration number is in the training step of GP model.  
525 Normally, the more iterations there are, the more accurate the result is. The  
526 result is presented in figure 11, where the horizontal axis indicates intervals of  
527 the predictive mean value  $\mu$  and the vertical axis indicates the number of testing  
528 data. A comparison of 20 and 40 iterations is carried out. Here the Coiflet 5 (C5)  
529 mother wavelet is chosen in the DWT and the first 512 coefficients are saved to  
530 be used as input for GP. Logistic function is chosen as the likelihood function and  
531 Variational Bayesian (VB) is selected as the inference method. The global mean  
532 value of predictive mean value for all testing damaged cases and that for healthy  
533 cases  $\mu_g = \frac{1}{n} \sum_{i=1}^n \mu_i$  are  $-0.891$  and  $0.667$  for 20 iterations, while the results for  
534 40 iterations are  $-0.885$  and  $0.775$  respectively. Besides, 1 case with ground truth  
535 (GT) 'healthy' is misclassified in the 'damaged' class for 20 iterations, while every

536 case is correctly classified with 40 iterations. Moreover, the class distance for 40  
537 iterations is larger than that for 20 iterations. It shows that with more iterations, the  
538 result is slightly better than with less iterations, which is consistent with common  
539 sense.

540 It should be noted that the current research is based on simulation, and in  
541 real experimental data the impact of environmental noise should be taken into  
542 consideration. Therefore, it is necessary to add noise to the simulation data to  
543 simulate the influence of environmental noise, so as to verify the stability of the  
544 proposed method. White Gaussian noise is added into the raw vibration data that  
545 are collected from sensors. Signal-noise ratio (SNR) is set as 20dB. Then the same  
546 procedure of signal processing with DWT and Gaussian Process classification is  
547 conducted. A comparison of classification result based on noise-free data and data  
548 with noise is illustrated in figure 12. Despite the added noise, the class distance has  
549 only slightly decreased, and all data can be correctly classified. This proves that  
550 the method proposed in this paper is still practical under simulated environmental  
551 noise.

## 552 5.2. Classification with one sensor

553 Now that an acceptable classification result has been obtained with a certain  
554 setup of the GP model using the data from 3 sensors, a discussion concerning  
555 the reduction of the number of sensors while ensuring the classification result is  
556 conducted.

557 Based on the results obtained in 5.1, the model configuration with mother  
558 wavelet C5, 256 DWT coefficients, Logistic likelihood function, VB inference  
559 method and 40 iterations is maintained. The pertinence of data from three sensors  
560 at different locations to the classification result is investigated. Data from three  
561 sensors are used for training and testing of the GP model independently. Results  
562 from the three GP models are compared between each other and also with the  
563 results with all data from sensor 1, 2 and 3, as shown in figure 13. It shows that  
564 with data from all three sensors the GP model achieves the best result in the current  
565 study. However, with data only from sensor 1, the classification accuracy can be  
566 100%, but it should be noted that as there exist several testing points so close to  
567 the threshold in both classes, they could probably be misclassified. With data only  
568 from sensor 3, at least 2 point among 81 are misclassified, but with data only from  
569 sensor 2 located at the diagonal of the actuator, the result is much worse where at  
570 least 6 testing points are misclassified.

571 In this section, Gaussian Process is evaluated by the data base collected  
572 through sensors attached on the sandwich plate. 70% of the database is used

573 for training and the rest 30% is used for testing. Several factors are evaluated  
574 successively and it is found that: to optimize hyperparameters during the training  
575 step, the more iterations, the better the results; during the signal processing and  
576 feature extraction, the mother wavelet Coiflet 5 in DWT is outperforming other  
577 mother wavelets; in the whole GP, the combination of Logistic function and Varia-  
578 tional Bayesian inference method is outstanding compared to other combinations;  
579 Reducing the amount of data by DWT will result in a slight loss of accuracy of  
580 the predictive mean value, but it can greatly reduce the computation time while  
581 ensuring the accuracy of classification, which is worthwhile for processing big data.  
582 Therefore, a GP model with mother wavelet C5, 256 DWT coefficients, Logistic  
583 likelihood function, VB inference method and 40 iterations is adopted in this study.  
584 The corresponding predictive mean values for healthy and damaged structure are  
585 0.800 and -0.870, respectively. As for the impact of the number of sensors, the  
586 result shows that data from sensor 1 and sensor 3 are more pertinent than that from  
587 sensor 2. It shows also that reducing of the number of sensors in the current study  
588 will lead to worse results.

## 589 6. Conclusions

590 This paper addresses the difficulty in constructing a database for structural  
591 health monitoring of real composite structures and the inconvenience in conven-  
592 tional expertise-based SHM approaches. A data-driven approach GP for damage  
593 detection in a composite sandwich plate by simulation approach is presented. Sev-  
594 eral factors that have impact on classification accuracy are investigated, including  
595 the selection of mother wavelet during the signal processing and feature extraction  
596 by DWT, the amount of data discarded by DWT, the likelihood function and infer-  
597 ence method that are used to make predictions, as well as iteration numbers in the  
598 training step of GP model. Based on the present results, some conclusions can be  
599 drawn as below:

- 600 ● The proposed method is proven effective for crack-type damage detection in  
601 the studied composite sandwich plate.
- 602 ● The selection of mother wavelet in discrete wavelet transform has an im-  
603 portant impact on the classification accuracy. Coiflet 5 performs better than  
604 others for the classification of both healthy and damaged structure.
- 605 ● Discarding the coefficients that have low amplitude in DWT can speed up  
606 the computation time and may not lead to major loss of information. **The**  
607 **resulted reduction of classification accuracy is negligible.**

- 608     • The likelihood function Logistic function and inference method Variational  
609       Bayesian perform better than other combinations in the present study.
- 610     • With more iterations, the classification is slightly better than with less itera-  
611       tions, which is consistent with common sense.
- 612     • Data from sensor 1 and sensor 3 are more pertinent than that from sensor 2.  
613       Reducing of the number of sensors in the current study will lead to worse  
614       results.
- 615     • **The effectiveness of the proposed method is verified under simulated envi-  
616       ronmental noise.**

617       **Although the proposed approach was achieved based on simulation results,  
618       it is applicable for real experimental data. The same procedure of data collection,  
619       signal processing and the use of GP model can be conducted as for simulation data  
620       for the purpose of damage detection.** This proposed method is capable to detect  
621       crack-type damages for a composite sandwich panel. It is expected to be suitable  
622       for damage detection of other kind of damages and for more complex structures.

### 623 **Acknowledgements**

624       Z. Liu is a PhD student supported by China Scholarship Council.

### 625 **Data availability**

626       The raw/processed data required to reproduce these findings cannot be shared  
627       at this time as the data also forms part of an ongoing study.

### 628 **References**

- 629     [1] D. Gay, Composite materials: design and applications, CRC press, 2014.
- 630     [2] D. Balageas, C. P. Fritzen, A. Güemes, Structural health monitoring, John  
631       Wiley & Sons, 2010.
- 632     [3] R. Lammering, U. Gabbert, M. Sinapius, T. Schuster, P. Wierach, Lamb-  
633       Wave Based Structural Health Monitoring in Polymer Composites, Springer  
634       International Publishing, 2017.

- 635 [4] C. Yang, S. O. Oyadiji, Delamination detection in composite laminate  
636 plates using 2d wavelet analysis of modal frequency surface, *Computers  
637 & Structures* 179 (2017) 109–126. doi:[https://doi.org/10.1016/  
638 j.compstruc.2016.10.019](https://doi.org/10.1016/j.compstruc.2016.10.019).
- 639 [5] K. Zhu, M. Chen, Q. Lu, B. Wang, D. Fang, Debonding detection of  
640 honeycomb sandwich structures using frequency response functions, *Jour-  
641 nal of Sound and Vibration* 333 (21) (2014) 5299 – 5311. doi:<https://doi.org/10.1016/j.jsv.2014.05.023>.
- 642 [6] Z. Huang, C. Zang, Damage detection using modal rotational mode shapes  
643 obtained with a uniform rate csldv measurement, *Applied Sciences* 9 (23)  
644 (2019) 4982.
- 645 [7] A. Katunin, Vibration-based spatial damage identification in honeycomb-core  
646 sandwich composite structures using wavelet analysis, *Composite Struc-  
647 tures* 118 (2014) 385 – 391. doi:[https://doi.org/10.1016/j.  
648 compstruct.2014.08.010](https://doi.org/10.1016/j.compstruct.2014.08.010).
- 649 [8] A. Katunin, H. Lopes, J. A. dos Santos, Identification of multiple damage  
650 using modal rotation obtained with shearography and undecimated wavelet  
651 transform, *Mechanical Systems and Signal Processing* 116 (2019) 725–740.
- 652 [9] J. Zhou, Z. Li, J. Chen, Damage identification method based on continuous  
653 wavelet transform and mode shapes for composite laminates with cutouts,  
654 *Composite Structures* 191 (2018) 12–23.
- 655 [10] N. D. A. Farrar C R, Doebling S W, Vibration-based structural damage  
656 identification, *Philosophical Transactions of the Royal Society of London  
657 A.* 359 (1778) (2001) 131–149. doi:[https://doi.org/10.1098/  
658 rsta.2000.0717](https://doi.org/10.1098/rsta.2000.0717).
- 659 [11] W. Bayissa, N. Haritos, S. Thelandersson, Vibration-based structural dam-  
660 age identification using wavelet transform, *Mechanical Systems and Signal  
661 Processing* 22 (5) (2008) 1194 – 1215. doi:[https://doi.org/10.  
662 1016/j.ymsp.2007.11.001](https://doi.org/10.1016/j.ymsp.2007.11.001).
- 663 [12] W. Weijtjens, T. Verbelen, E. Capello, C. Devriendt, Vibration based struc-  
664 tural health monitoring of the substructures of five offshore wind turbines,  
665 *Procedia engineering* 199 (2017) 2294–2299. doi:[https://doi.org/  
666 10.1016/j.proeng.2017.09.187](https://doi.org/10.1016/j.proeng.2017.09.187).
- 667

- 668 [13] D. Montalvao, N. M. M. Maia, A. M. R. Ribeiro, A review of vibration-based  
669 structural health monitoring with special emphasis on composite materi-  
670 als, *Shock and vibration digest* 38 (4) (2006) 295–324. doi:[10.1177/  
671 0583102406065898](https://doi.org/10.1177/0583102406065898).
- 672 [14] Y. Zou, L. Tong, G. P. Steven, Vibration-based model-dependent damage  
673 (delamination) identification and health monitoring for composite struc-  
674 tures—a review, *Journal of Sound and vibration* 230 (2) (2000) 357–378.  
675 doi:[10.1006/jsvi.1999.2624](https://doi.org/10.1006/jsvi.1999.2624).
- 676 [15] S. W. Doebling, C. R. Farrar, M. B. Prime, et al., A summary review of  
677 vibration-based damage identification methods, *Shock and vibration digest*  
678 30 (2) (1998) 91–105.
- 679 [16] X. Yu, M. Ratssepp, Z. Fan, Damage detection in quasi-isotropic composite  
680 bends using ultrasonic feature guided waves, *Composites Science and Tech-  
681 nology* 141 (2017) 120 – 129. doi:[https://doi.org/10.1016/j.  
682 compscitech.2017.01.011](https://doi.org/10.1016/j.compscitech.2017.01.011).
- 683 [17] P. Aryan, A. Kotousov, C.-T. Ng, B. Cazzolato, A model-based method  
684 for damage detection with guided waves, *Structural Control and Health  
685 Monitoring* 24 (3) (2017) e1884. doi:[10.1002/stc.1884](https://doi.org/10.1002/stc.1884).
- 686 [18] S. Sikdar, S. Banerjee, Identification of disbond and high density core region  
687 in a honeycomb composite sandwich structure using ultrasonic guided waves,  
688 *Composite Structures* 152 (2016) 568 – 578. doi:[https://doi.org/  
689 10.1016/j.compstruct.2016.05.064](https://doi.org/10.1016/j.compstruct.2016.05.064).
- 690 [19] M. Mitra, S. Gopalakrishnan, Guided wave based structural health monitoring:  
691 A review, *Smart Materials and Structures* 25 (5) (2016) 053001. doi:[10.  
692 1088/0964-1726/25/5/053001](https://doi.org/10.1088/0964-1726/25/5/053001).
- 693 [20] N. Chakraborty, V. Rathod, D. R. Mahapatra, S. Gopalakrishnan, Guided  
694 wave based detection of damage in honeycomb core sandwich structures,  
695 *NDT & E International* 49 (2012) 27 – 33. doi:[https://doi.org/10.  
696 1016/j.ndteint.2012.03.008](https://doi.org/10.1016/j.ndteint.2012.03.008).
- 697 [21] F. Song, G. L. Huang, K. Hudson, Guided wave propagation in honeycomb  
698 sandwich structures using a piezoelectric actuator/sensor system, *Smart Mate-  
699 rials and Structures* 18 (12) (2009) 125007. doi:[10.1088/0964-1726/  
700 18/12/125007](https://doi.org/10.1088/0964-1726/18/12/125007).

- 701 [22] S. Thwaites, N. Clark, Non-destructive testing of honeycomb sandwich struc-  
702 tures using elastic waves, *Journal of Sound and Vibration* 187 (2) (1995) 253  
703 – 269. doi:<https://doi.org/10.1006/jsvi.1995.0519>.
- 704 [23] C. Willberg, S. Duczec, J. M. Vivar-Perez, Z. A. B. Ahmad, Simulation Meth-  
705 ods for Guided Wave-Based Structural Health Monitoring: A Review, *Applied*  
706 *Mechanics Reviews* 67 (1) (01 2015). doi:[10.1115/1.4029539](https://doi.org/10.1115/1.4029539).
- 707 [24] Z. Su, L. Ye, Y. Lu, Guided lamb waves for identification of damage in  
708 composite structures: A review, *Journal of sound and vibration* 295 (3-5)  
709 (2006) 753–780. doi:[https://doi.org/10.1016/j.jsv.2006.](https://doi.org/10.1016/j.jsv.2006.01.020)  
710 [01.020](https://doi.org/10.1016/j.jsv.2006.01.020).
- 711 [25] M. Radzienski, M. Cao, X. Wei, P. Kudela, W. Ostachowicz, Combined vibra-  
712 tion and guided wave-based approach for composite panels health assessment,  
713 in: T. Kundu (Ed.), *Health Monitoring of Structural and Biological Systems*  
714 2017, Vol. 10170, International Society for Optics and Photonics, SPIE, 2017,  
715 pp. 499 – 506. doi:[10.1117/12.2260425](https://doi.org/10.1117/12.2260425).
- 716 [26] S. J. Russell, P. Norvig, *Artificial intelligence: a modern approach*, Malaysia;  
717 Pearson Education Limited, 2016.
- 718 [27] M. A. Torres-Arredondo, D. A. Tibaduiza-Burgos, An acousto-ultrasonics  
719 approach for probabilistic modelling and inference based on gaussian pro-  
720 cesses, *Structural Control and Health Monitoring* 25 (6) (2018) e2178.  
721 doi:<https://doi.org/10.1002/stc.2178>.
- 722 [28] C. M. Bishop, *Pattern recognition and machine learning*, springer, 2006.
- 723 [29] D. Tibaduiza, L. Mujica, J. Rodellar, Damage classification in structural  
724 health monitoring using principal component analysis and self-organizing  
725 maps, *Structural Control and Health Monitoring* 20 (10) (2013) 1303–1316.  
726 doi:<https://doi.org/10.1002/stc.1540>.

## 727 **Figure Captions**

728 Figure 1: Example of a DWT for a signal collected at sensor 2 (on the diagonal  
729 of the actuator)

730 Figure 2: Gaussian Process training step

731 Figure 3: Gaussian Process testing step

732 Figure 4a: Geometry of the composite sandwich panel

733 Figure 4b: Numerical model of the composite sandwich panel

734 Figure 5: Composite sandwich models with crack damage in different posi-  
735 tions: (a) in x direction  $x = \frac{L}{4}, y = \frac{W}{4}$  (b) in x direction  $x = \frac{L}{4}, y = \frac{W}{2}$  (c) in x  
736 direction  $x = \frac{L}{2}, y = \frac{W}{4}$  (d) in x direction  $x = \frac{L}{2}, y = \frac{W}{2}$  (e) in x direction  $x = \frac{3L}{4},$   
737  $y = \frac{3W}{4}$  (f) in y direction  $x = \frac{L}{2}, y = \frac{W}{2}$ . 1 actuator (red) and 3 sensors (yellow)  
738 attached on the face-sheet.

739 Figure 6: Comparison of structural vibration responses of a healthy model  
740 and a model with crack damage to an excitation signal of frequency 8 kHz.

741 Figure 7: Comparison of DWT coefficients of the vibration responses in  
742 Figure 6

743 Figure 8: Influence of the selection of mother wavelet on the classification  
744 accuracy

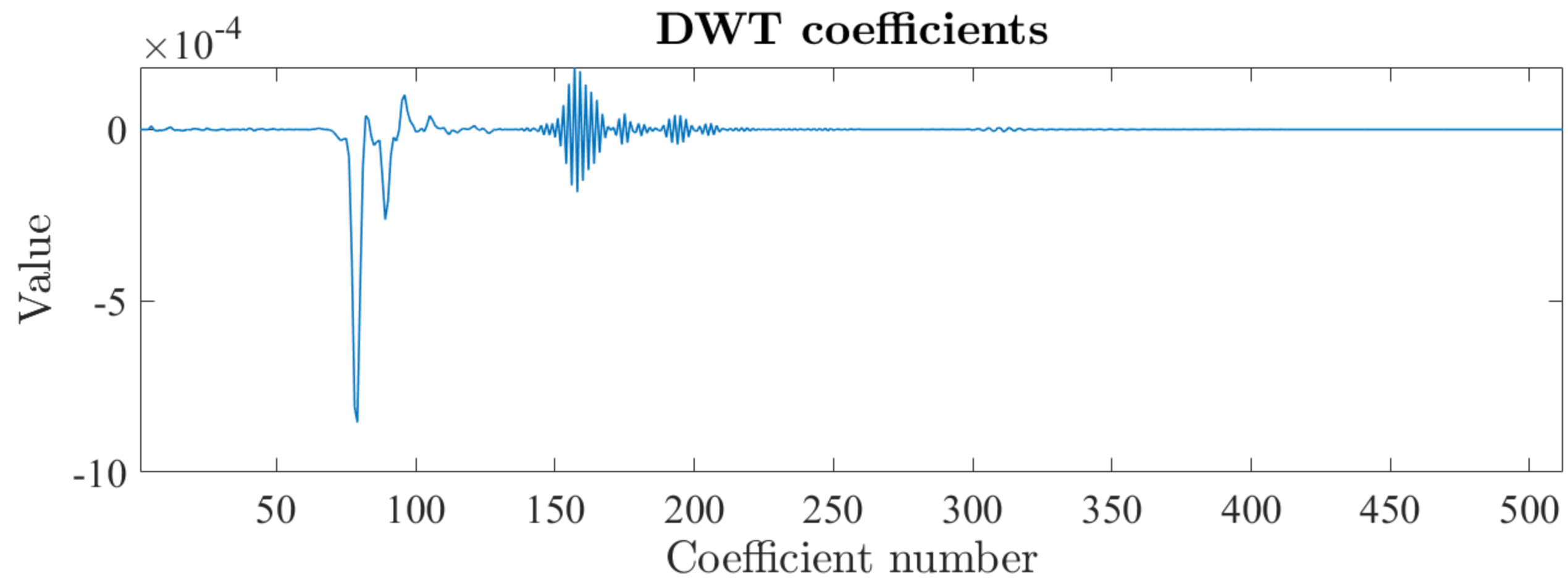
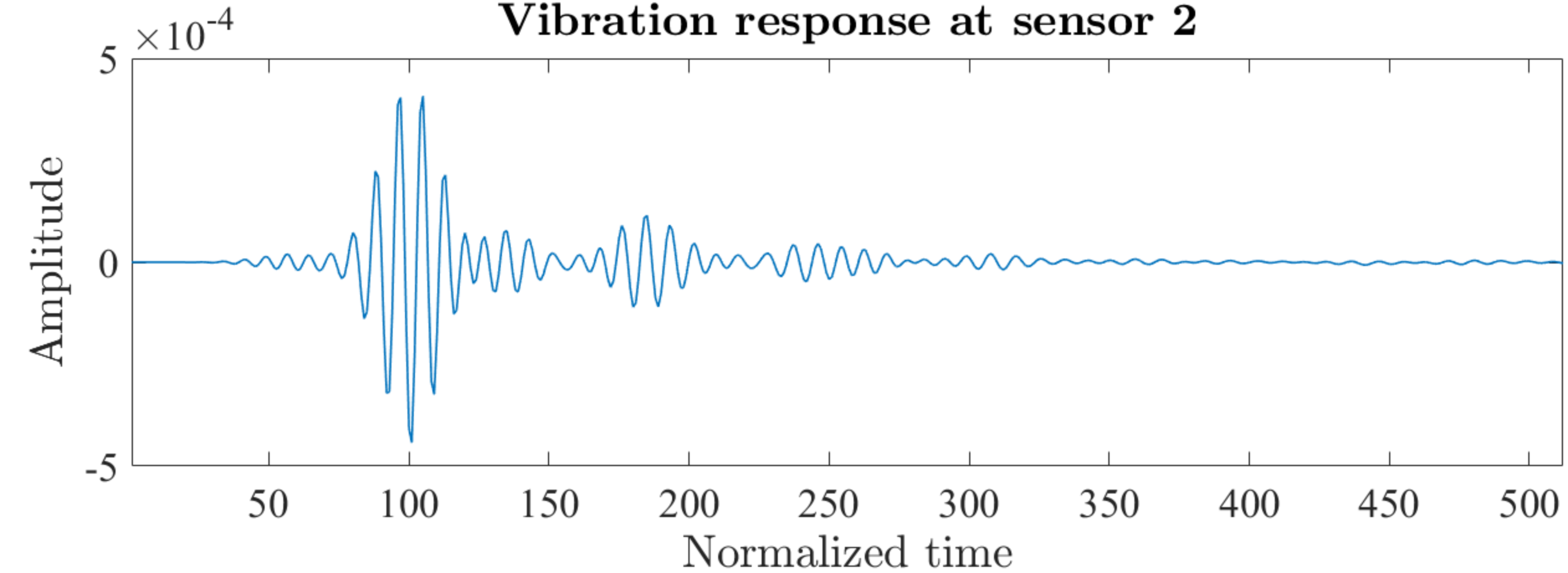
745 Figure 9: Influence of the amount of data saved by DWT on the classification  
746 accuracy

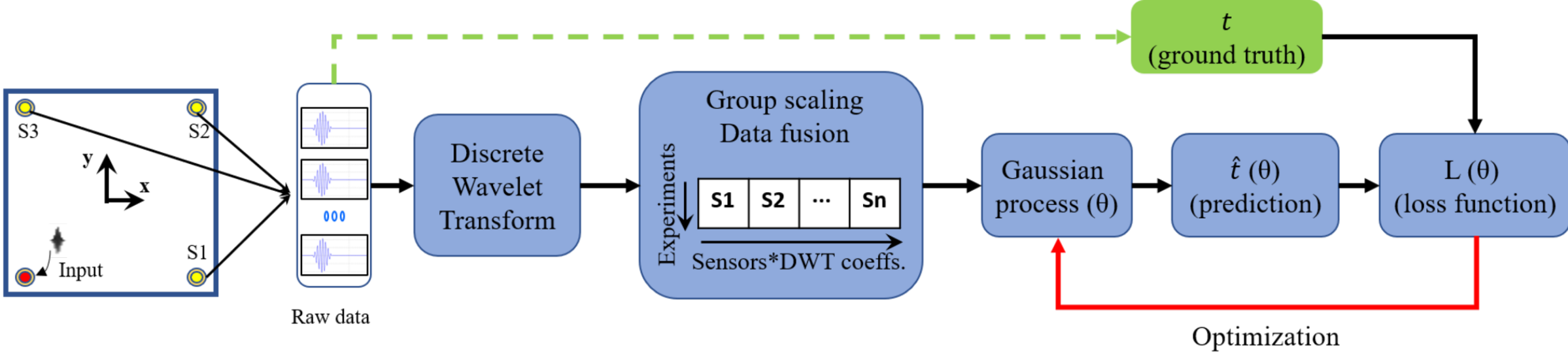
747 Figure 10: Influence of likelihood function and inference method on the  
748 classification accuracy

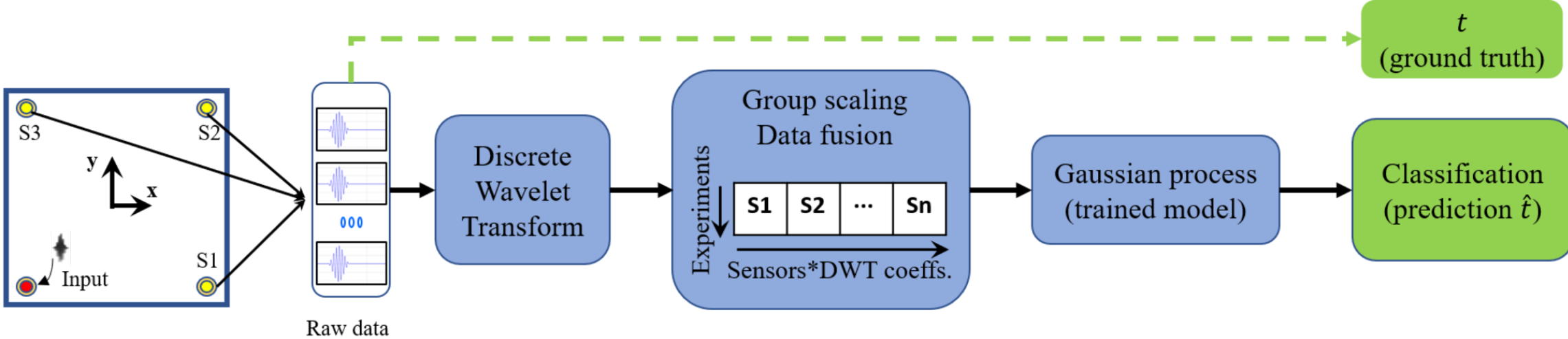
749 Figure 11: Influence of iteration numbers to optimize hyperparameters during  
750 the training step on the classification accuracy

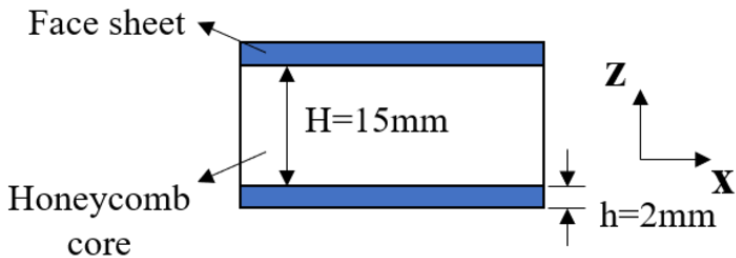
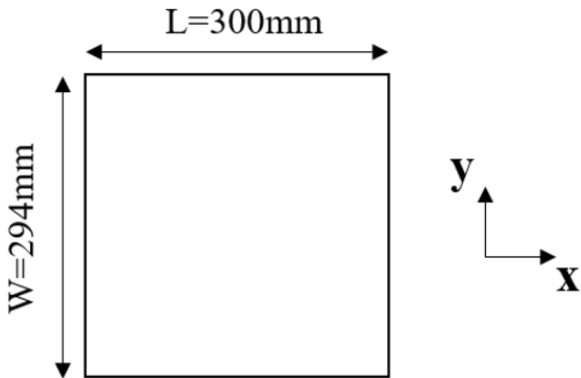
751 **Figure 12: Comparison of classification result based on (a) noise-free data**  
752 **and (b) data with noise**

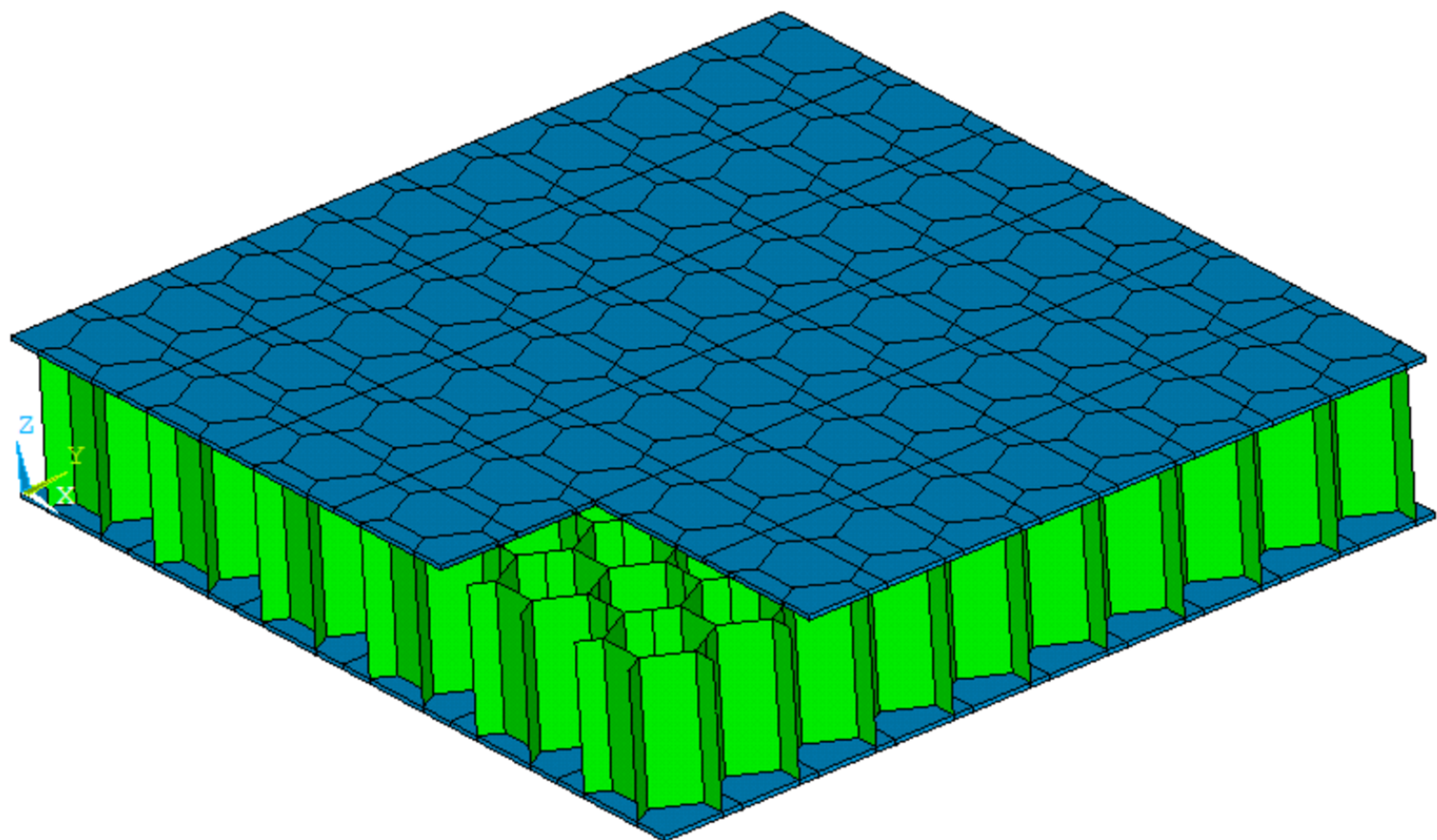
753 Figure 13: Investigation of the pertinence of three different sensors to the  
754 classification result. Classification using data only from sensor 1 (a), data only  
755 from sensor 2 (b), data only from sensor 3 (c) and data from sensor 1-3 (d)

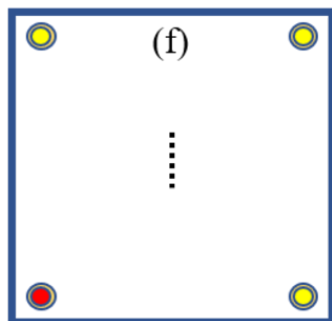
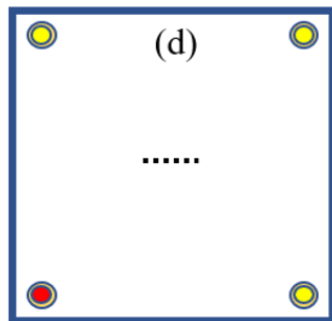
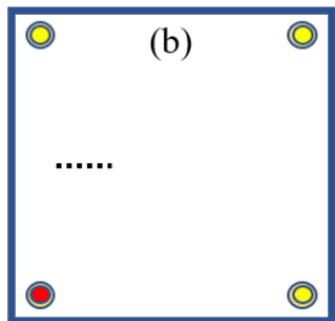
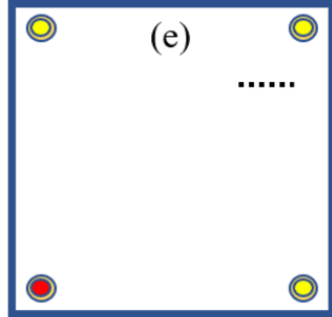
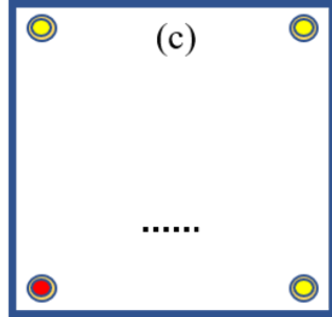
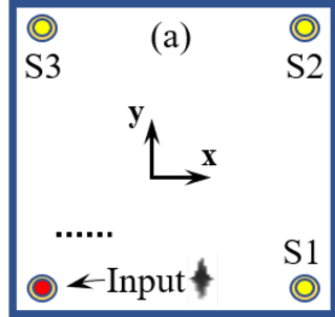


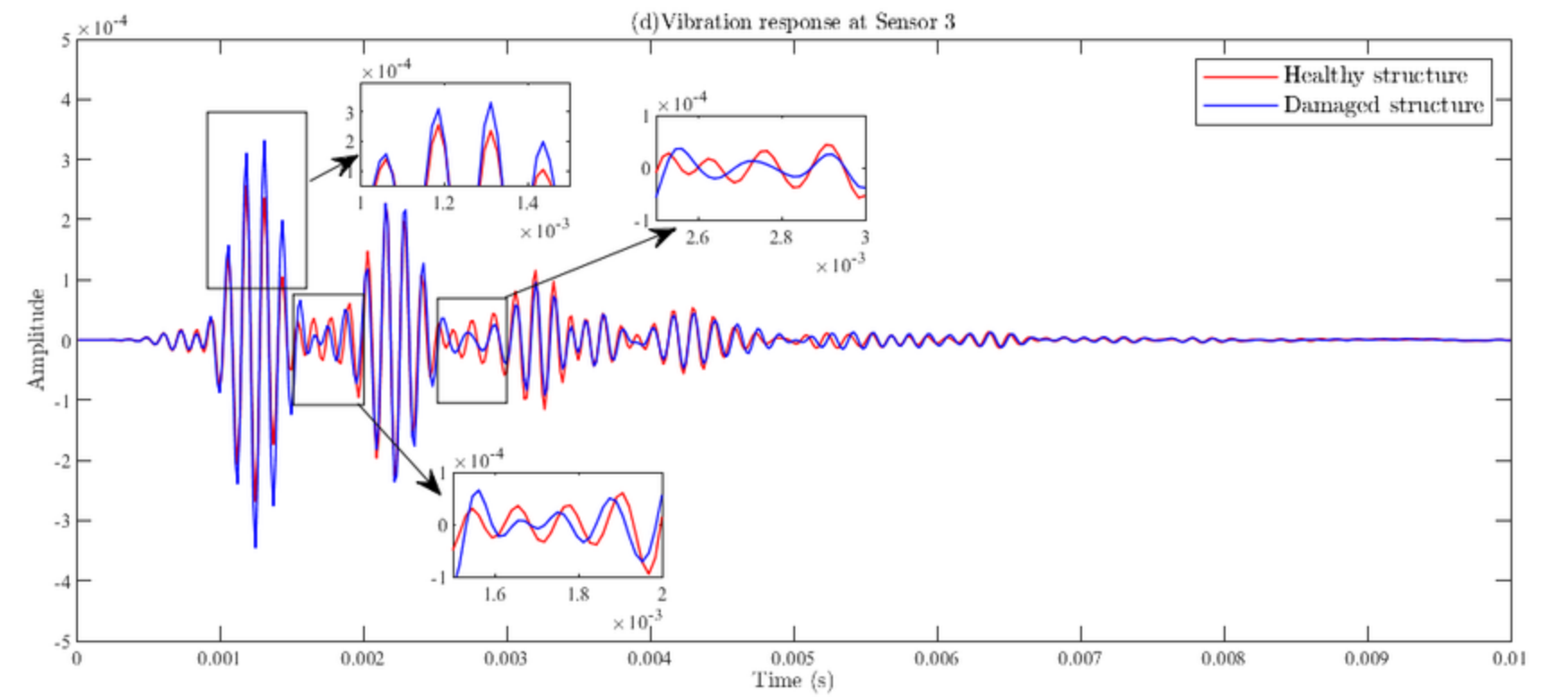
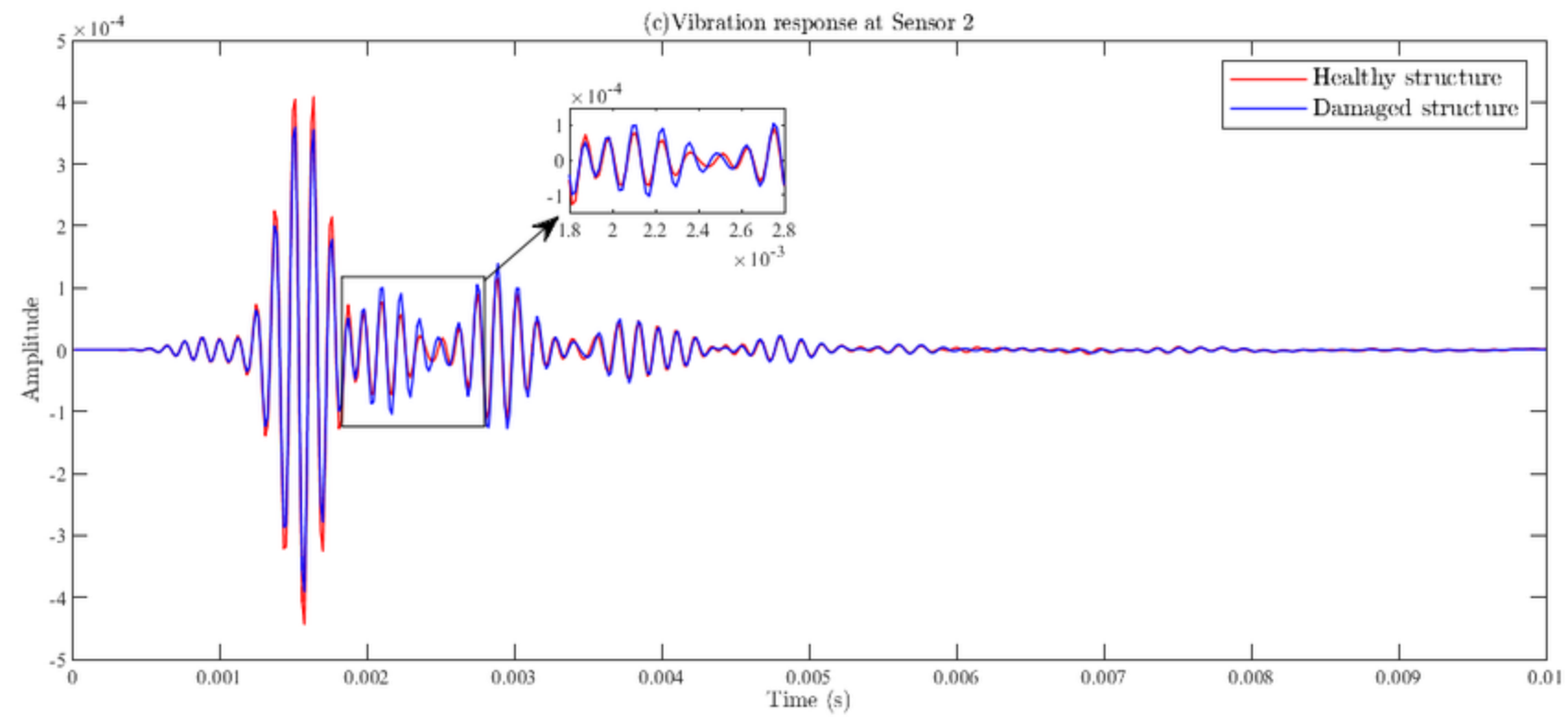
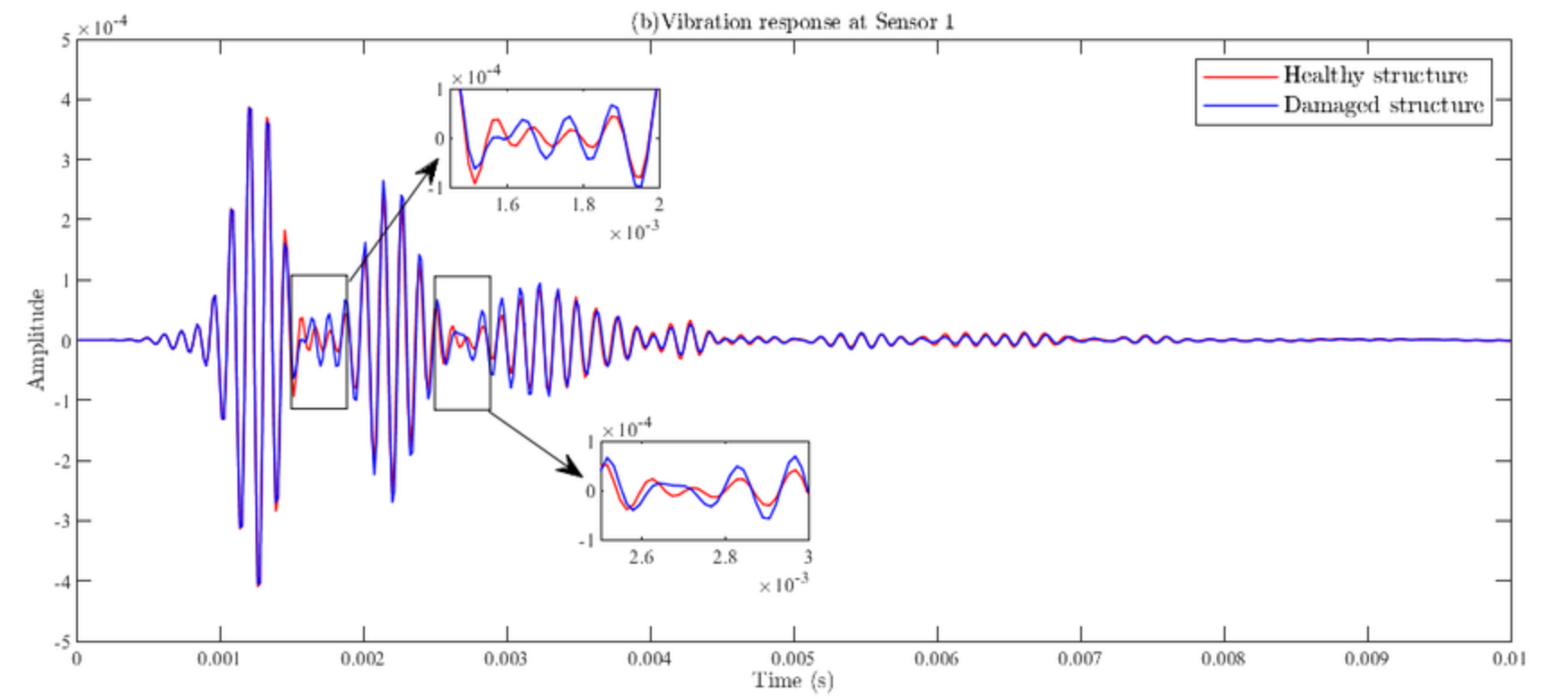
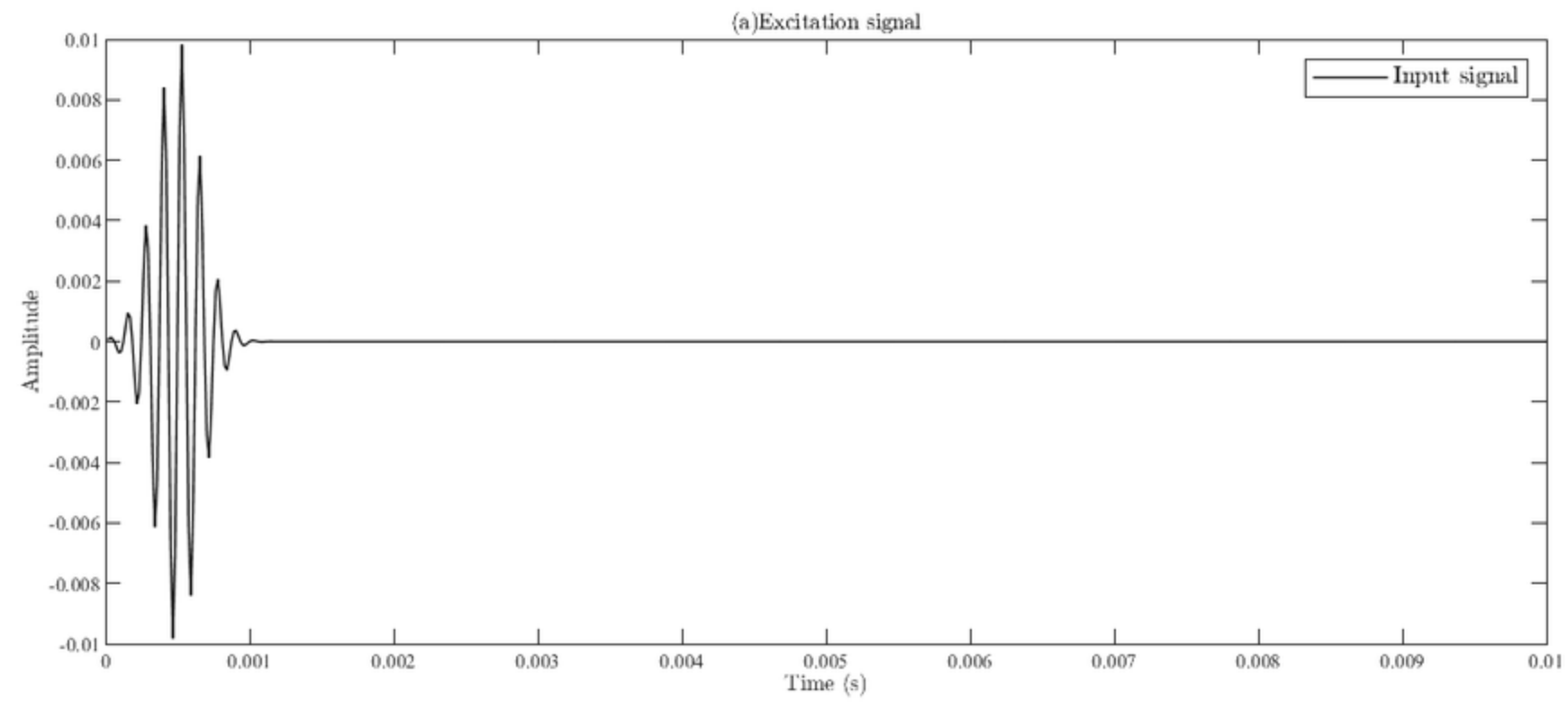




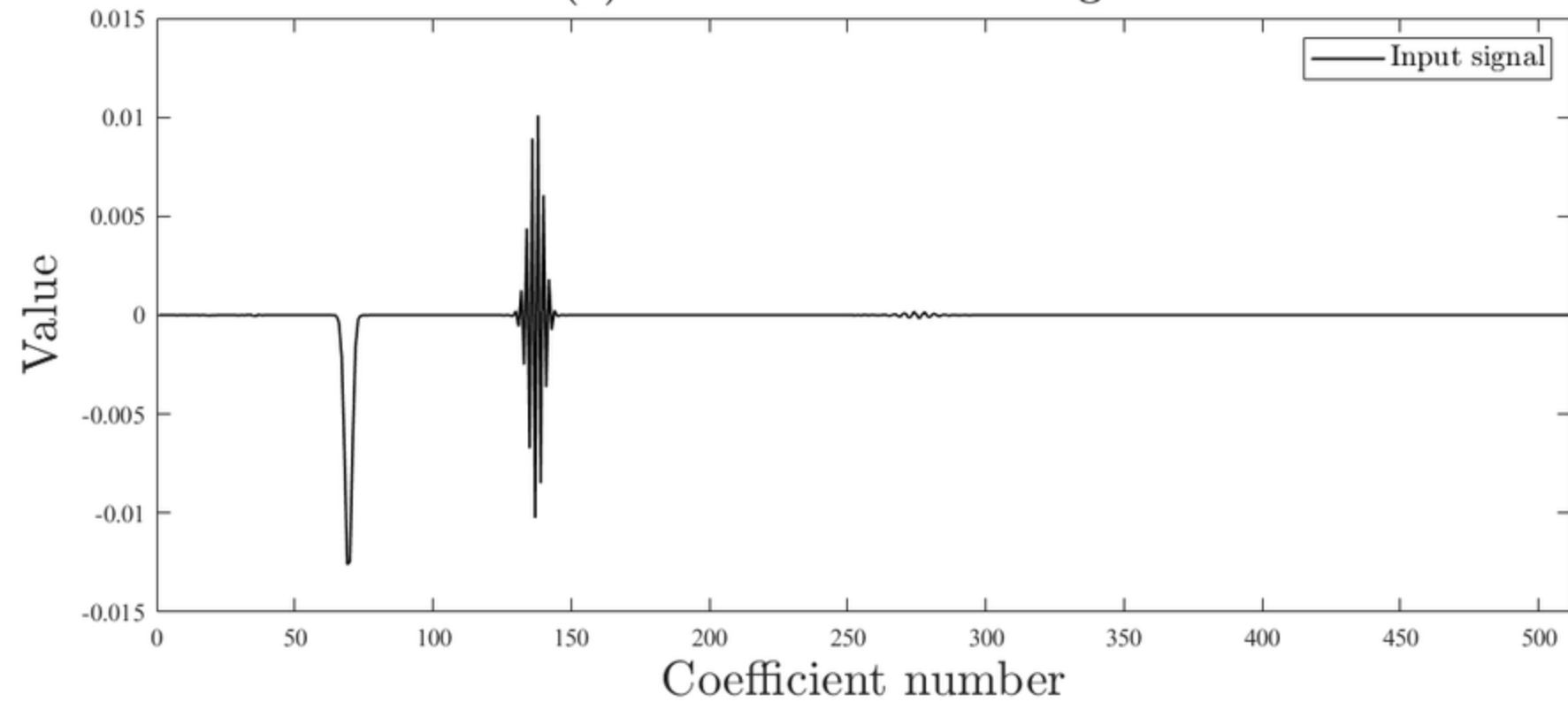




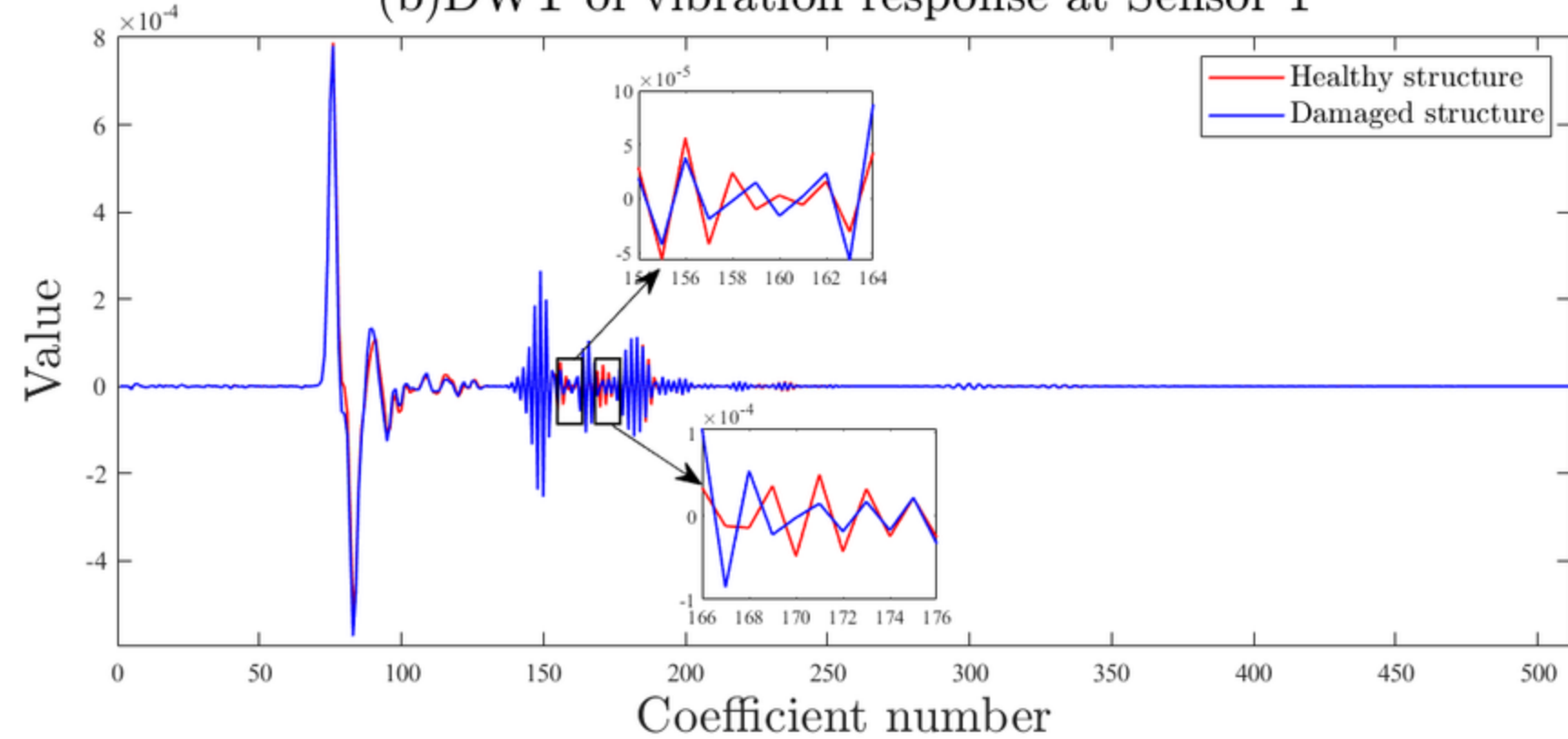




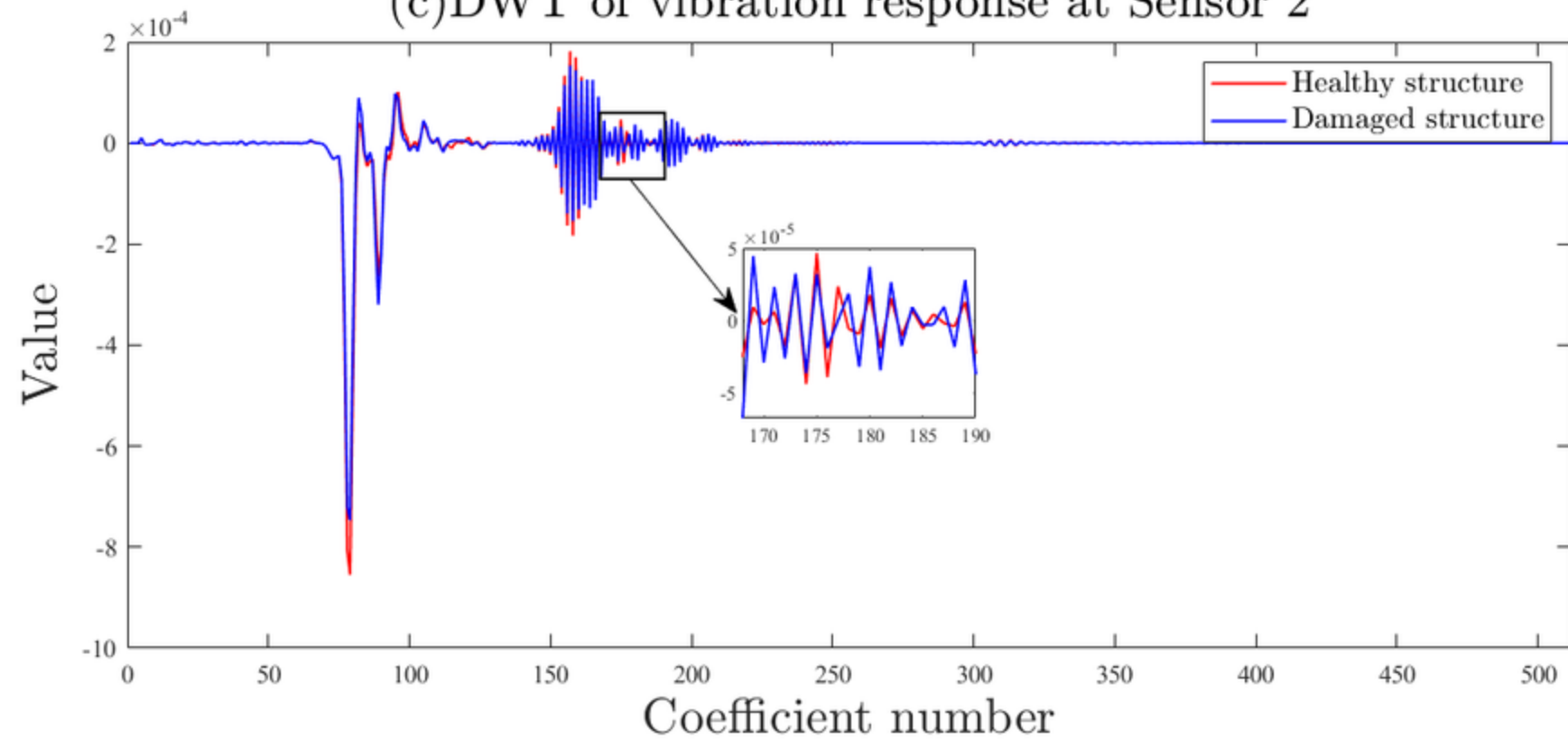
(a) DWT of excitation signal



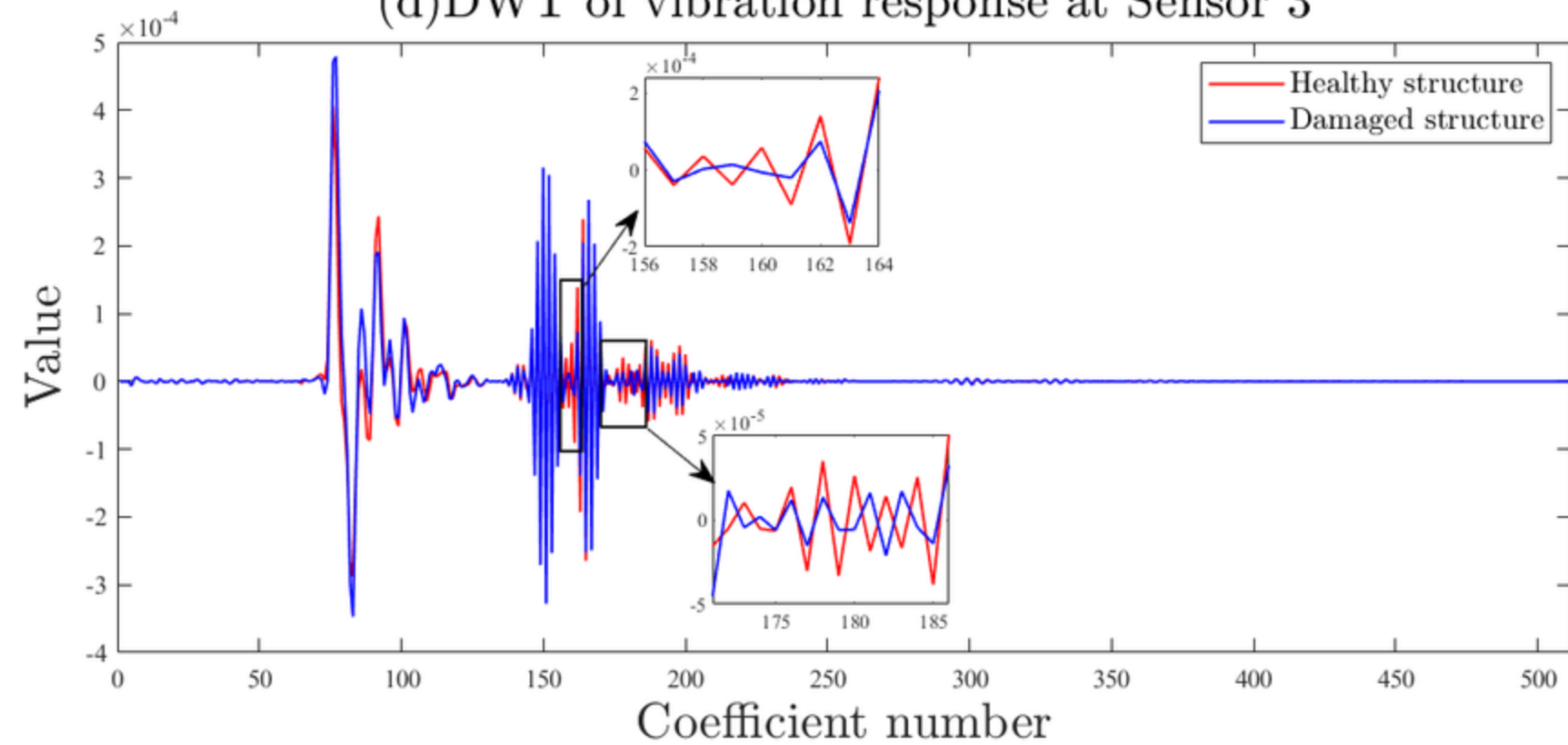
(b) DWT of vibration response at Sensor 1



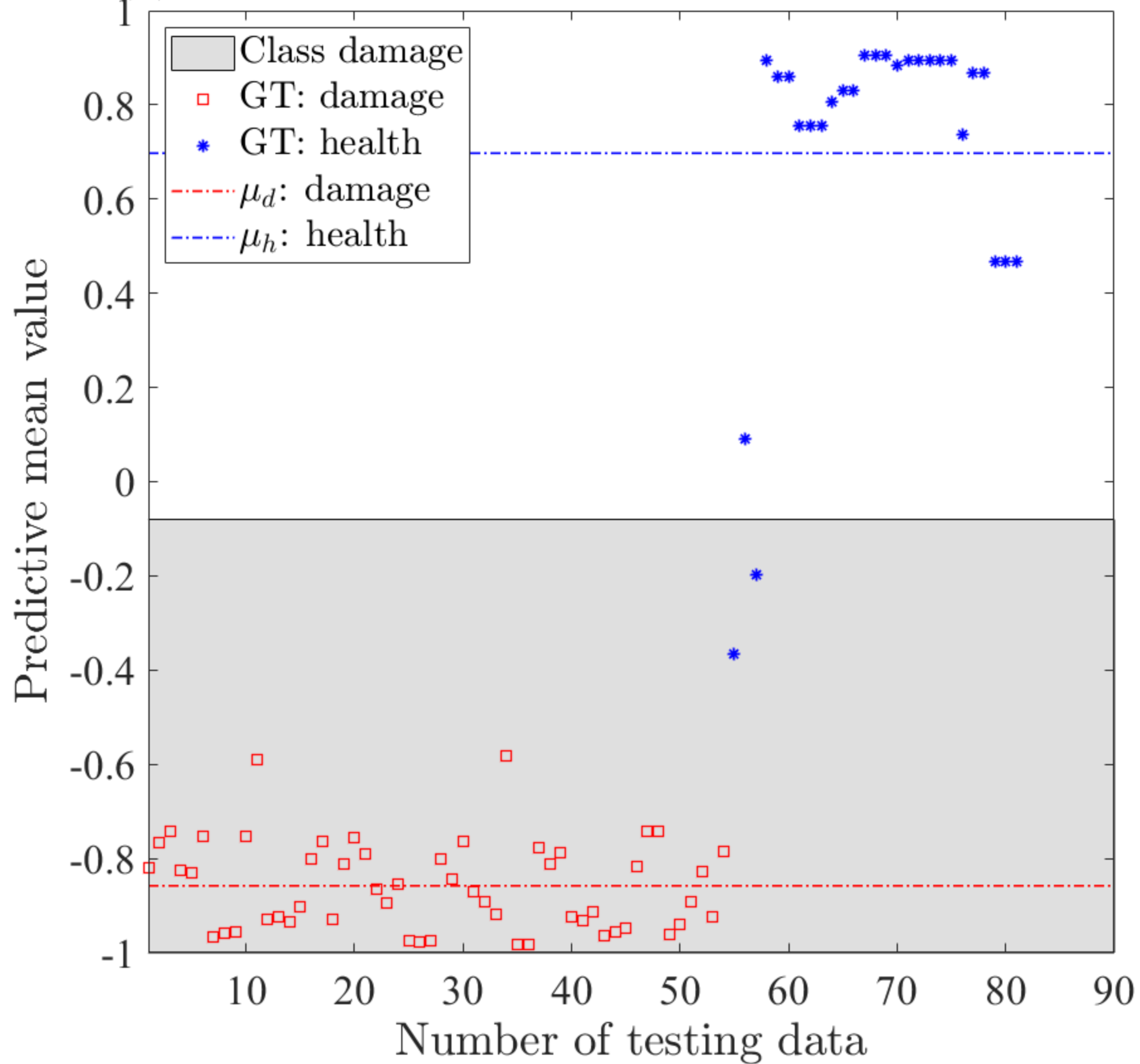
(c) DWT of vibration response at Sensor 2



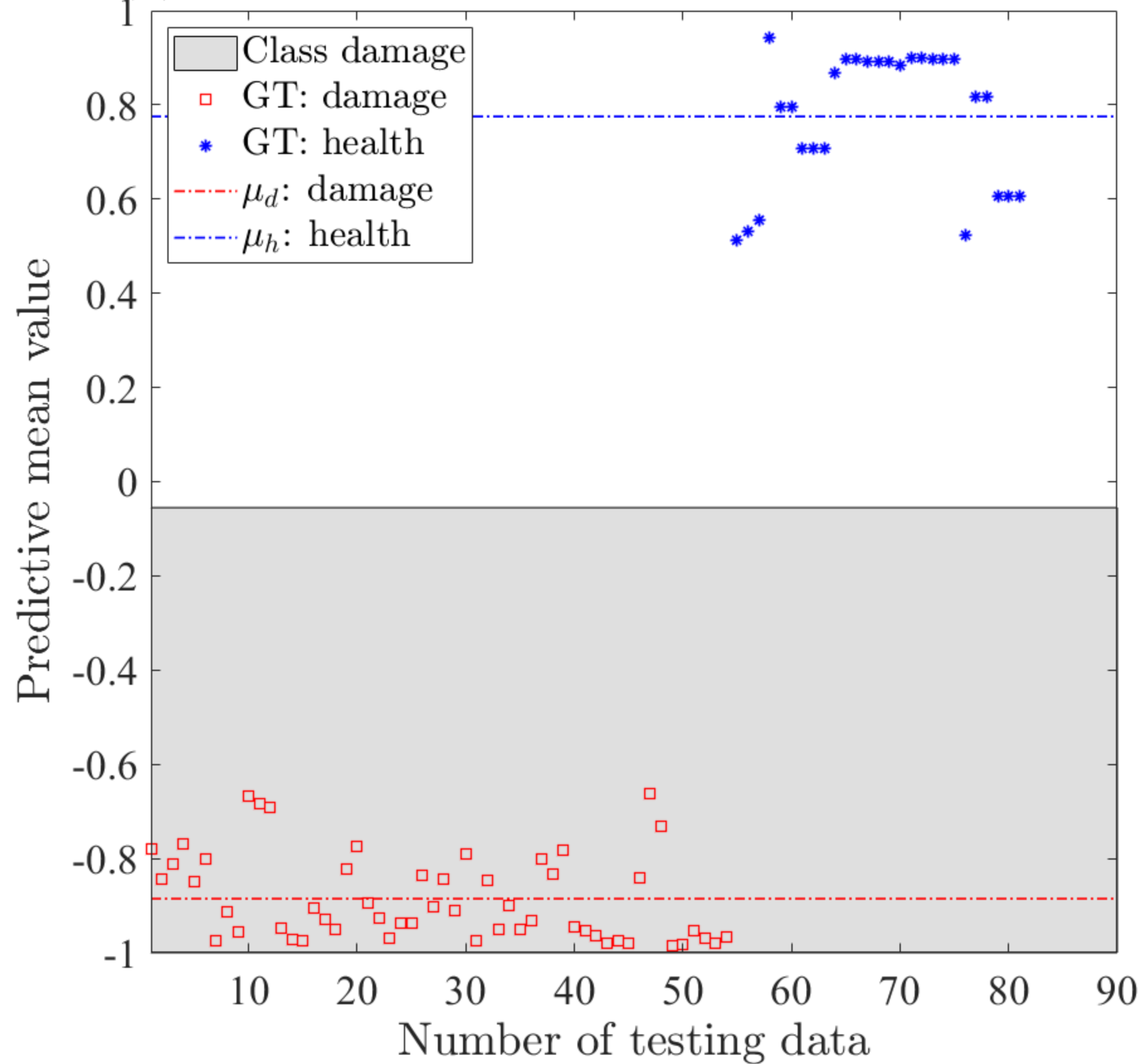
(d) DWT of vibration response at Sensor 3



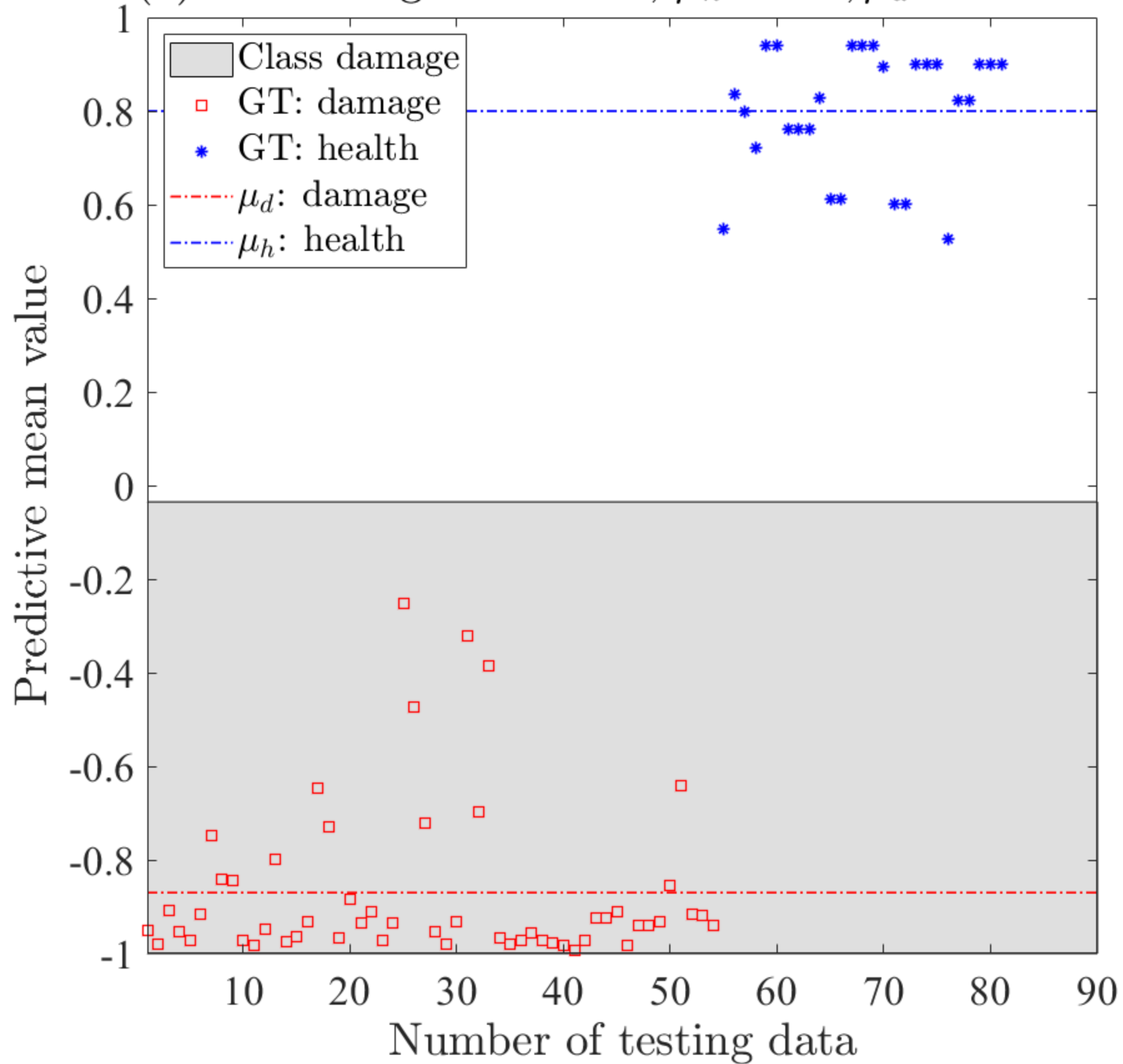
(a) D8-512-Logistic-VB-40,  $\mu_h = 0.697$ ,  $\mu_d = -0.858$



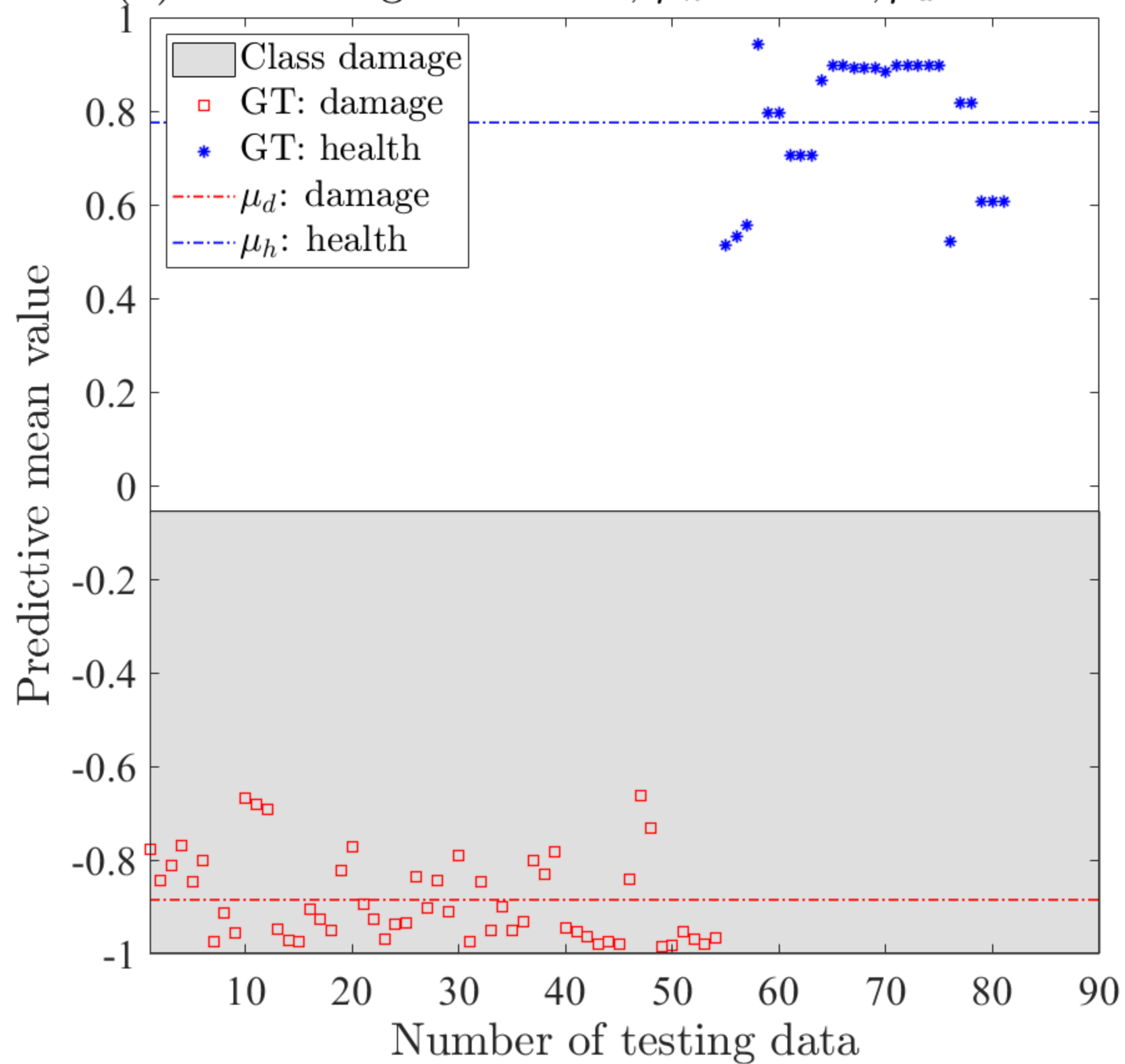
(b) C5-512-Logistic-VB-40,  $\mu_h = 0.775$ ,  $\mu_d = -0.885$



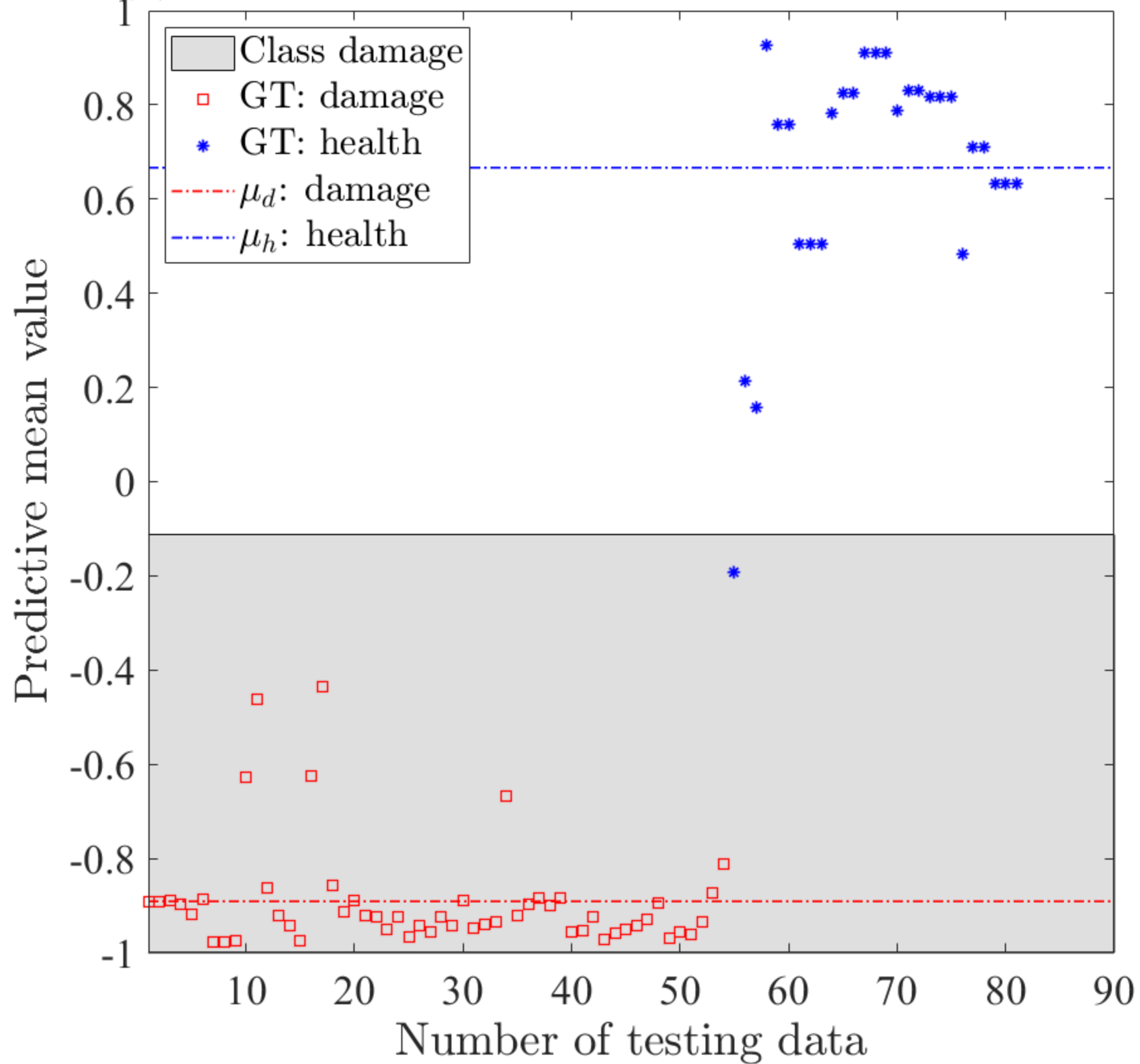
(a) C5-256-Logistic-VB-40,  $\mu_h = 0.8, \mu_d = -0.870$



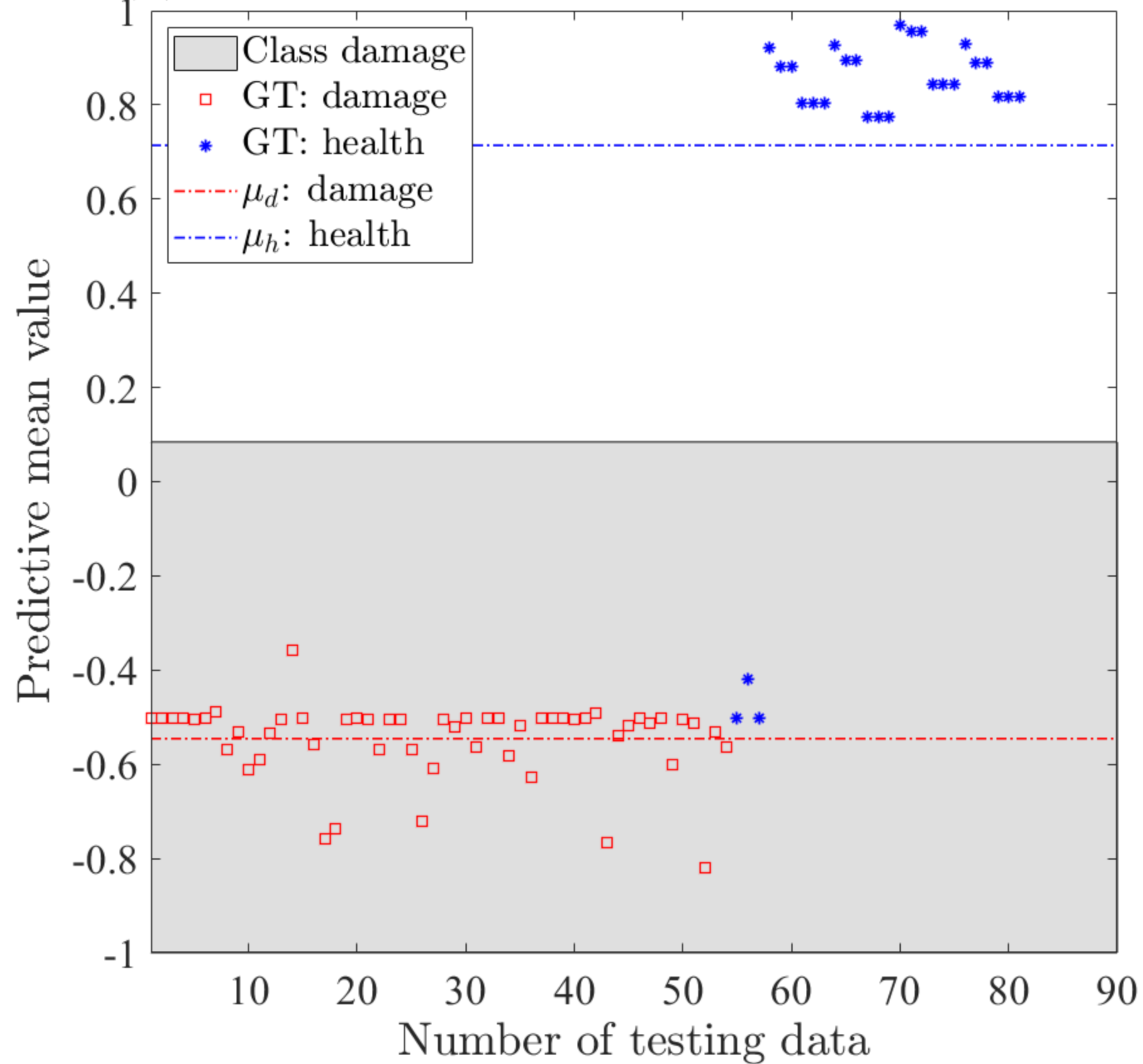
(b) C5-512-Logistic-VB-40,  $\mu_h = 0.775, \mu_d = -0.885$



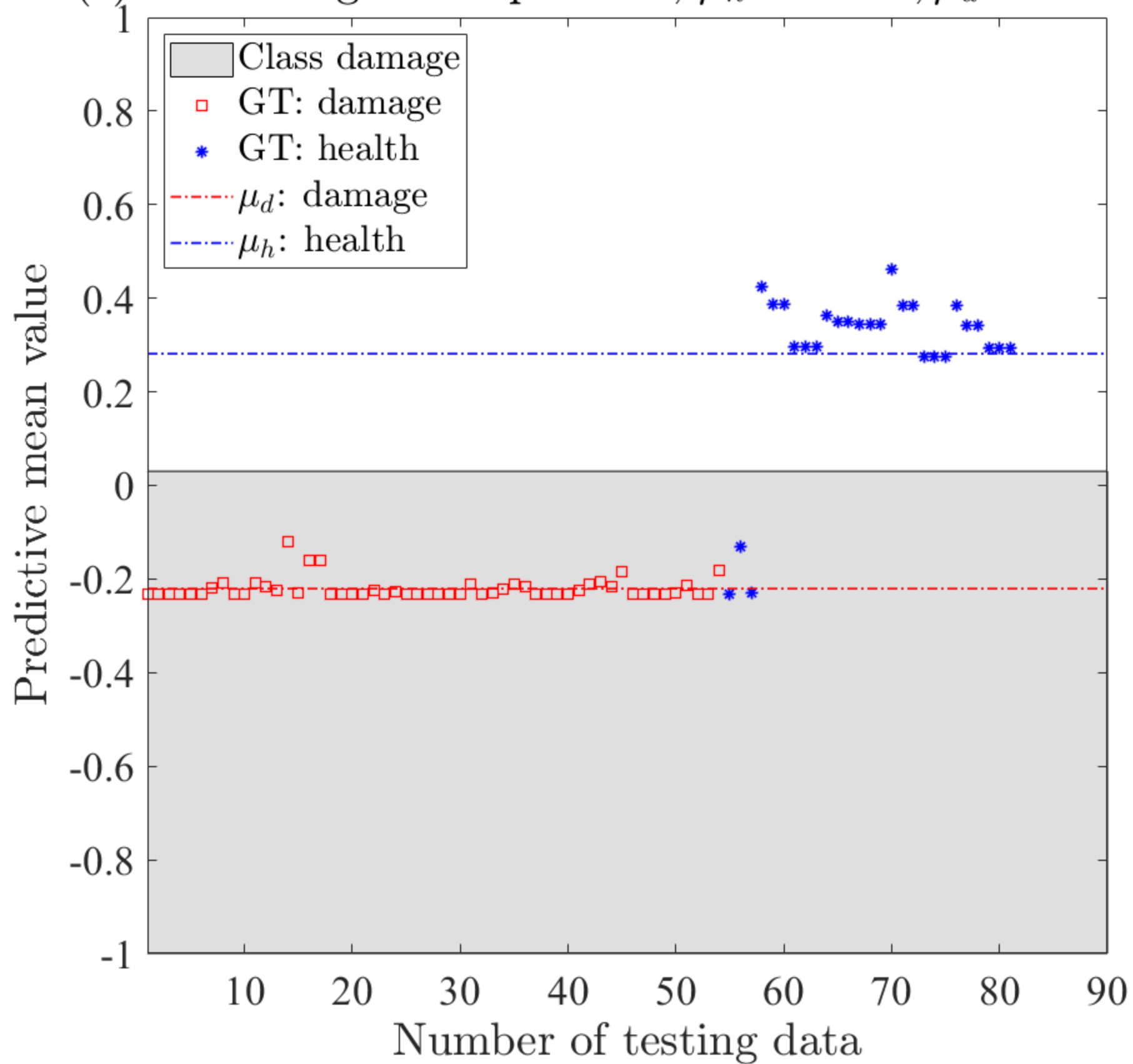
(a) C5-512-Logistic-VB-20,  $\mu_h = 0.667$ ,  $\mu_d = -0.891$



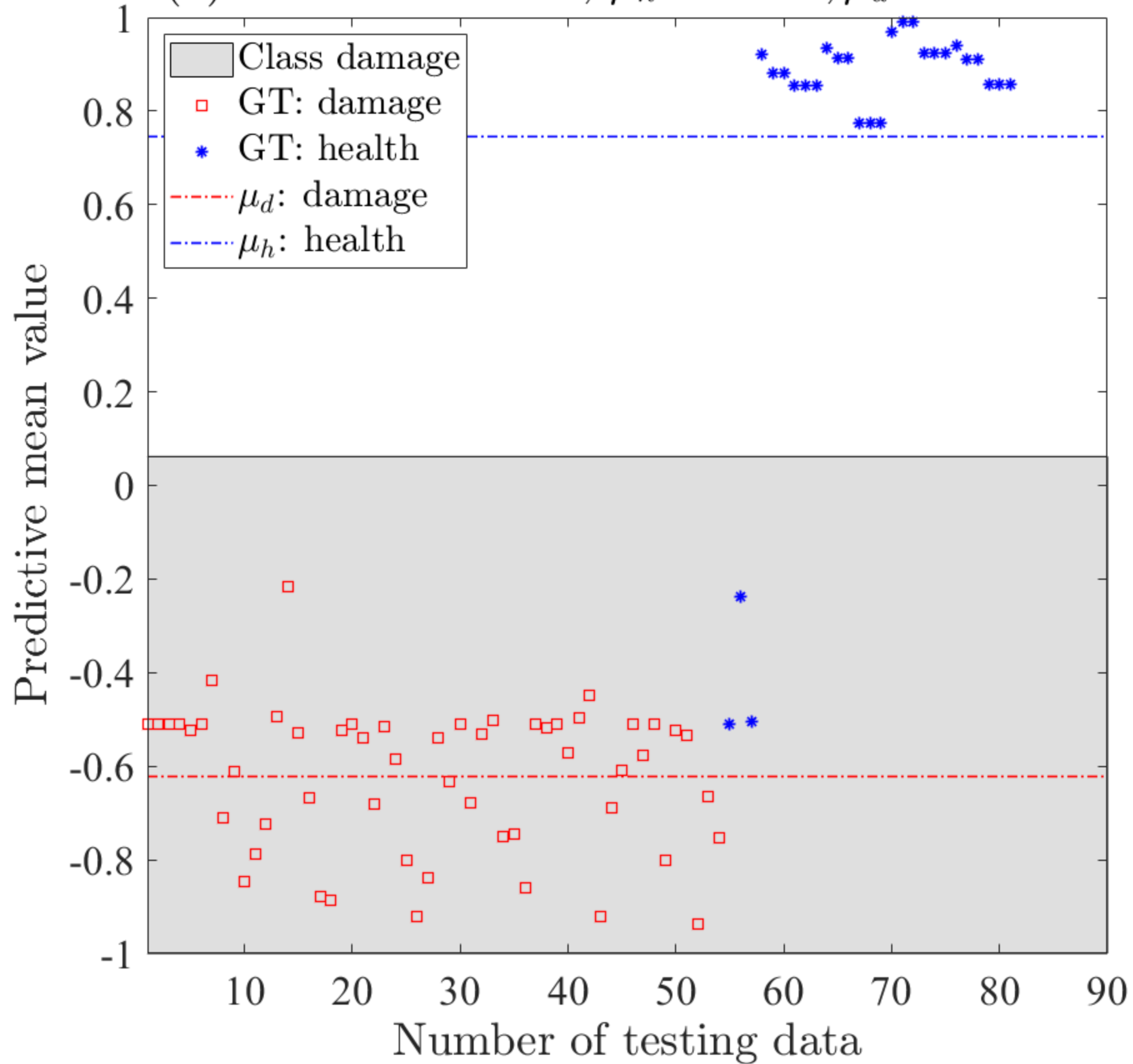
(b) C5-512-Logistic-EP-20,  $\mu_h = 0.714$ ,  $\mu_d = -0.546$



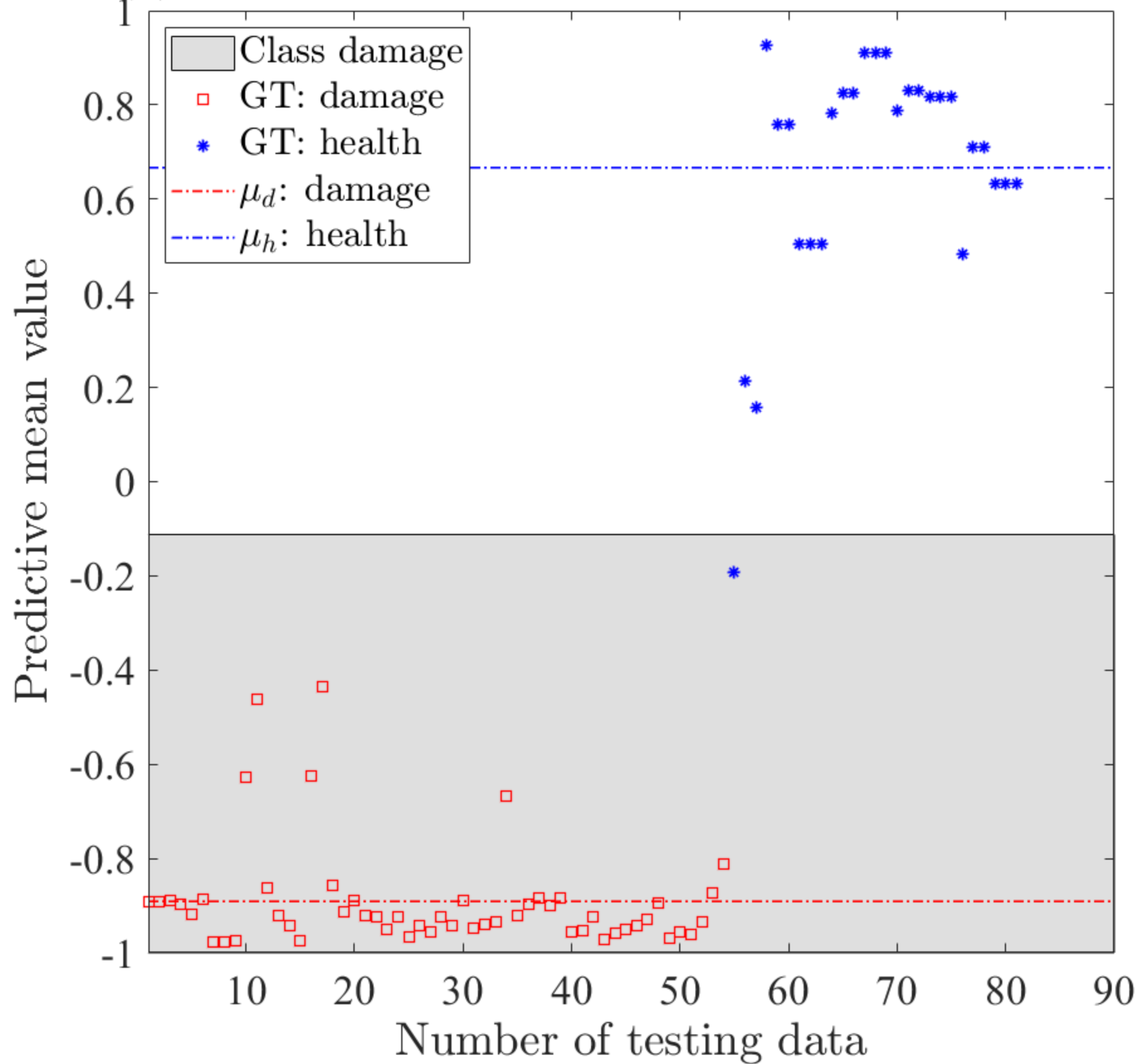
(c) C5-512-Logistic-Laplace-20,  $\mu_h = 0.281$ ,  $\mu_d = -0.220$



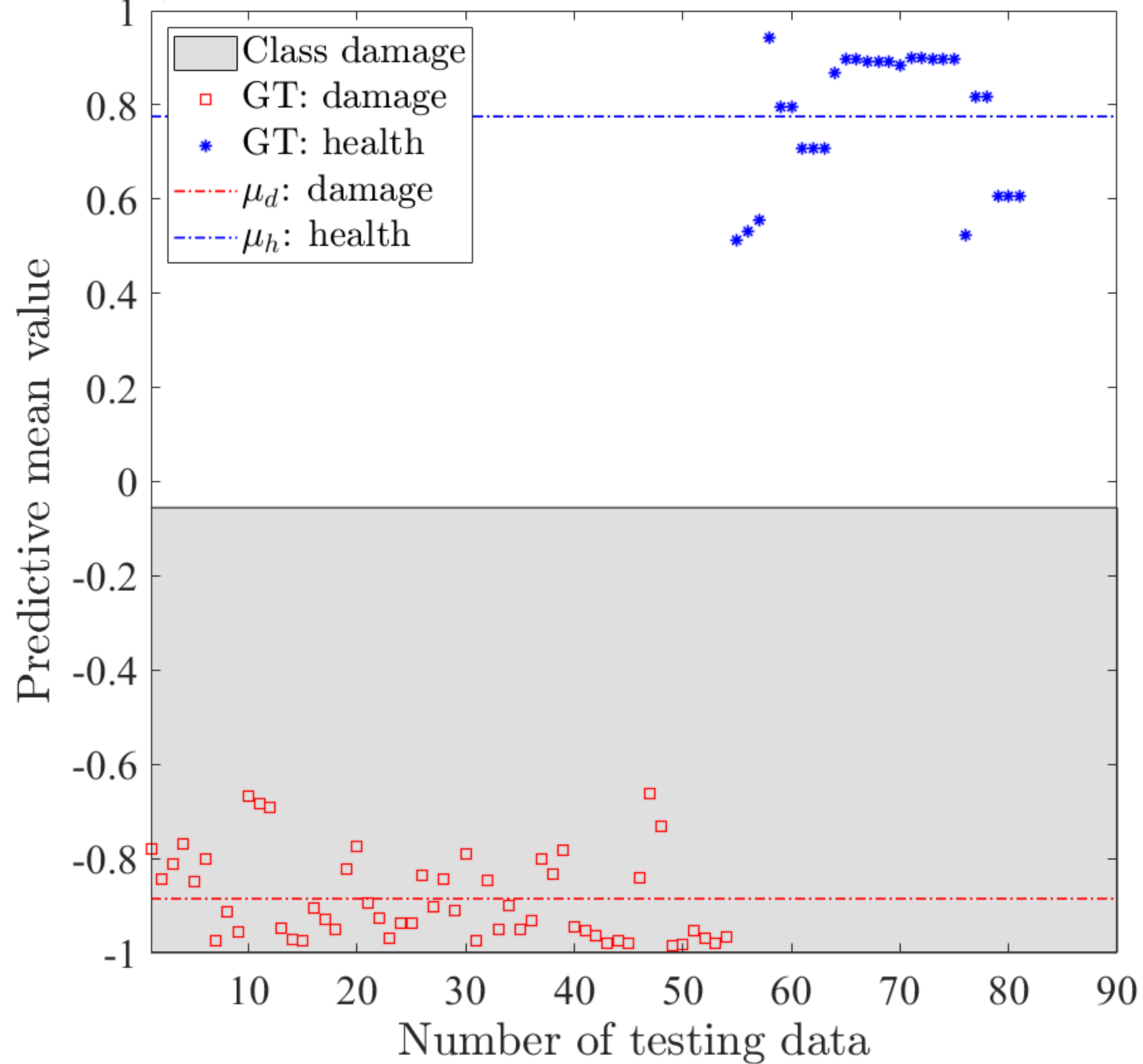
(d) C5-512-Erf-EP-20,  $\mu_h = 0.745$ ,  $\mu_d = -0.622$



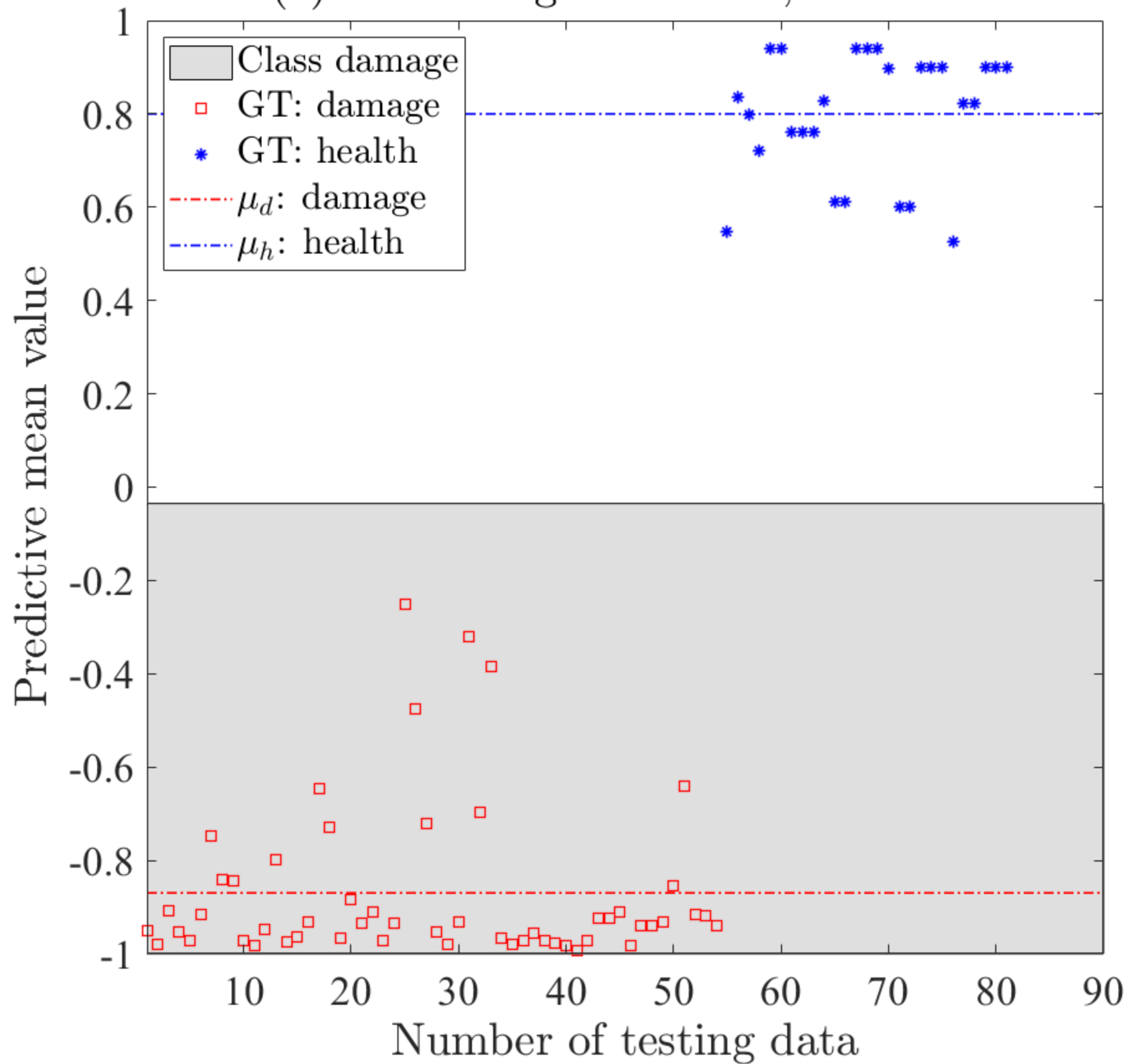
(a) C5-512-Logistic-VB-20,  $\mu_h = 0.667, \mu_d = -0.891$



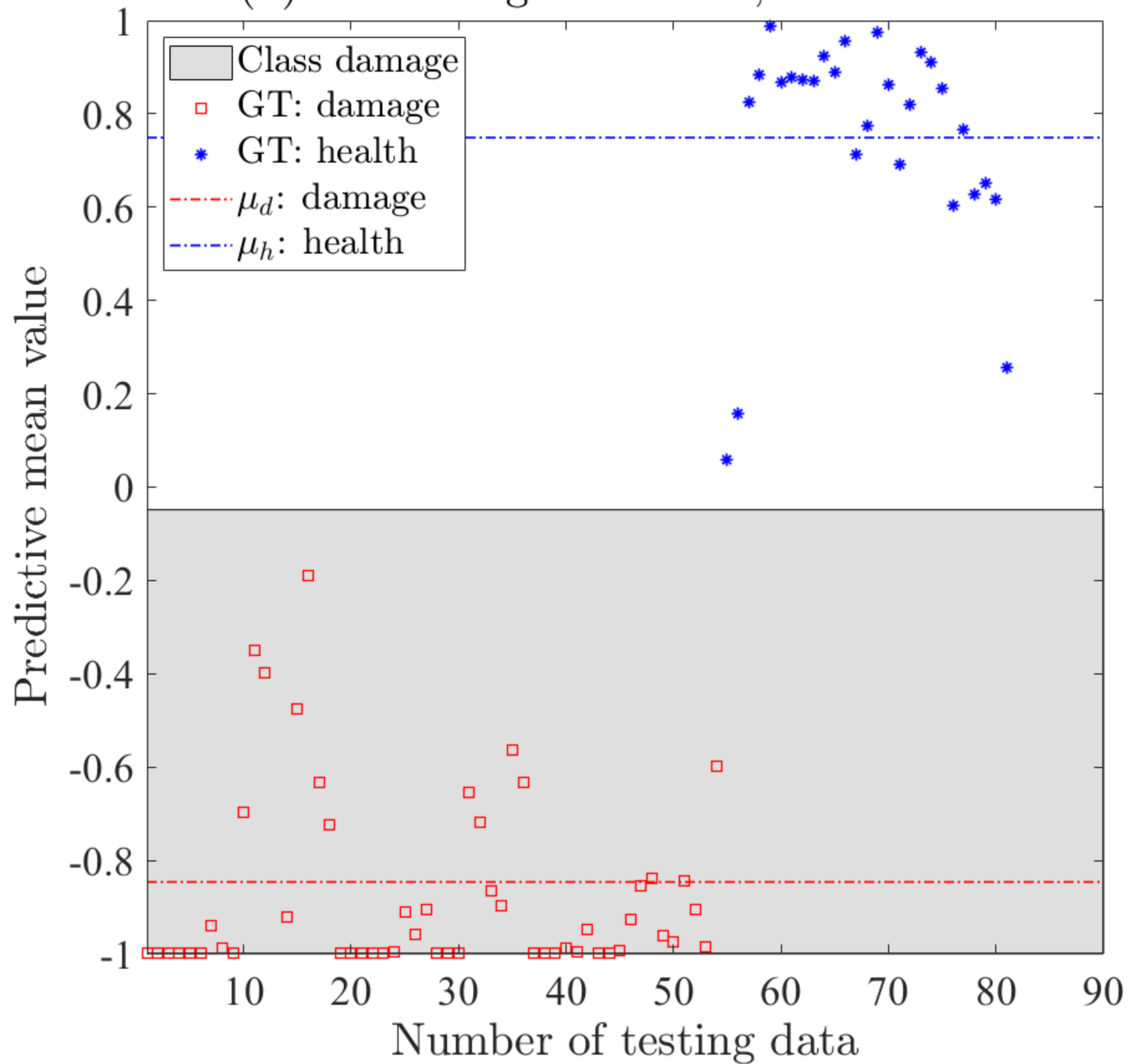
(b) C5-512-Logistic-VB-40,  $\mu_h = 0.775, \mu_d = -0.885$



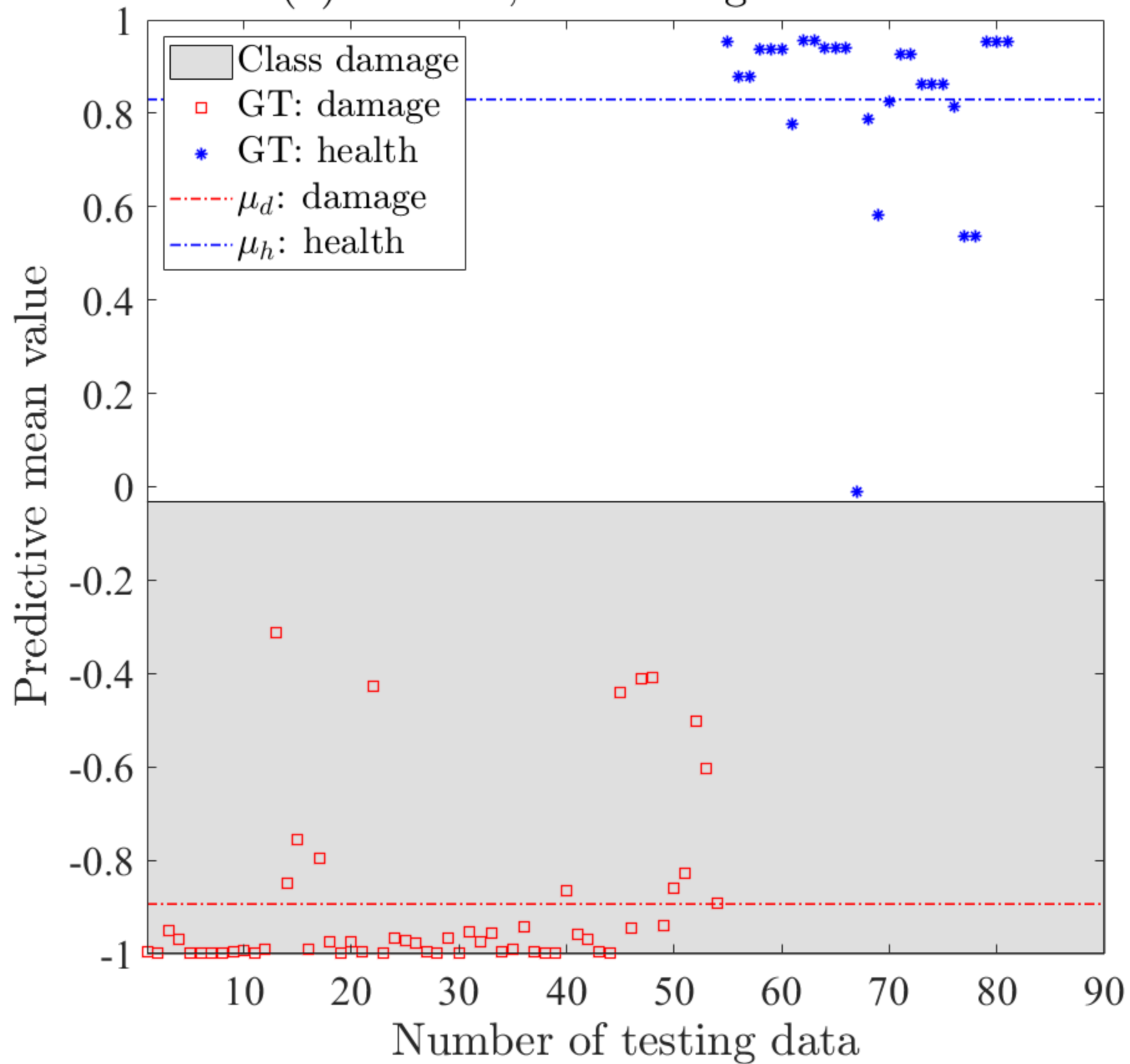
(a) C5-256-Logistic-VB-40, noise-free



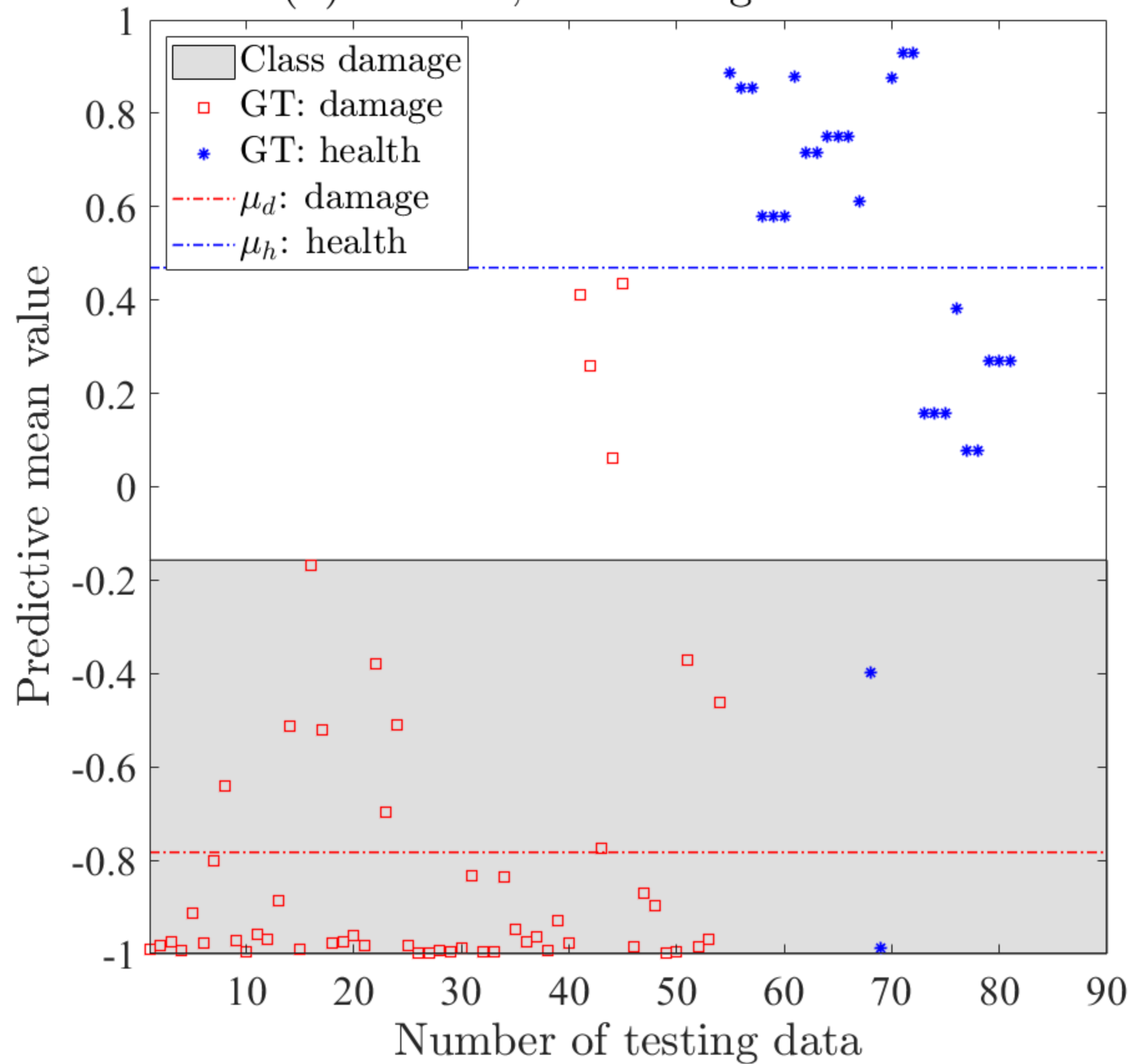
(b) C5-256-Logistic-VB-40, SNR=20dB



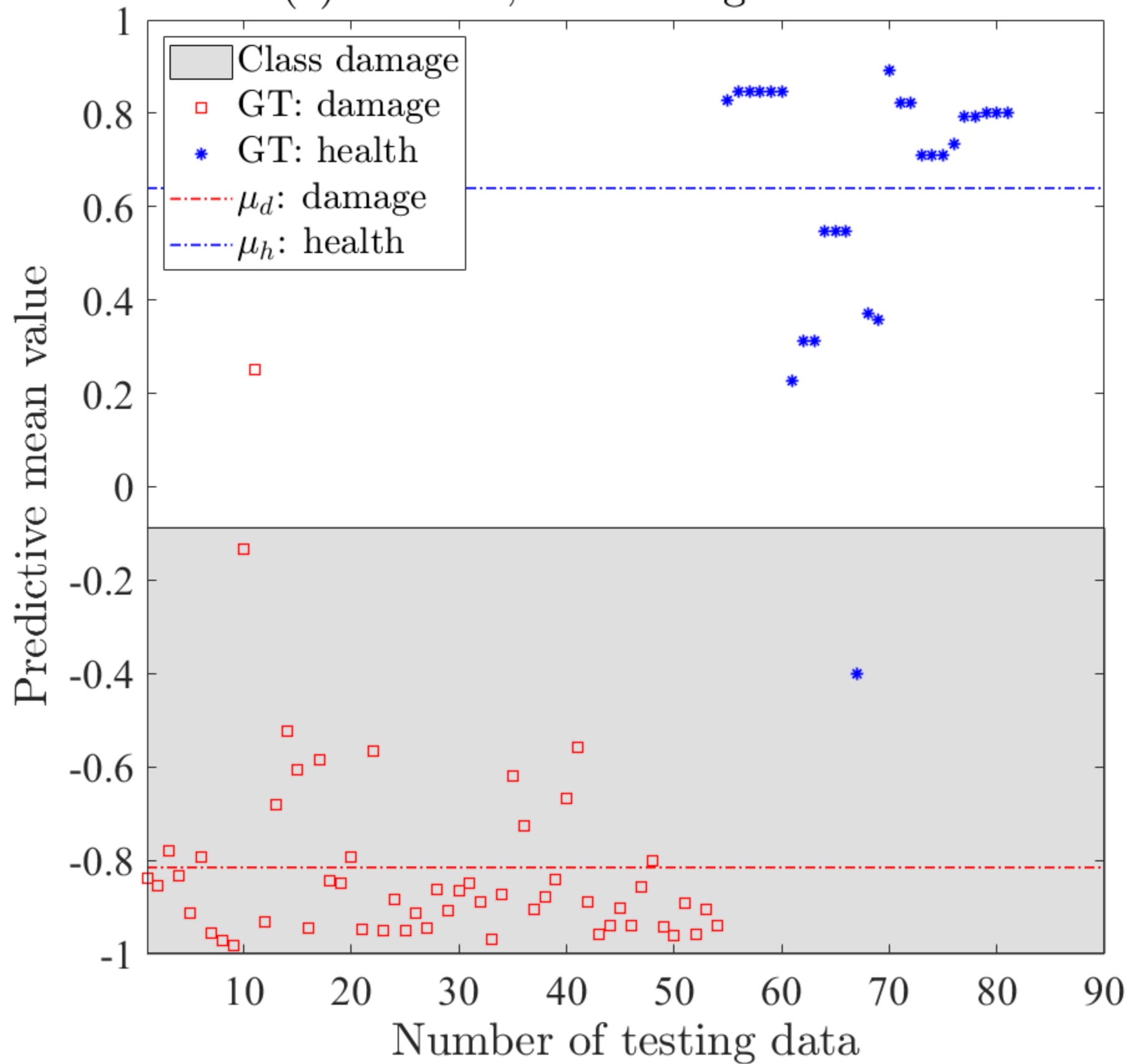
(a) Sensor 1, C5-256-Logistic-VB-40



(b) Sensor 2, C5-256-Logistic-VB-40



(c) Sensor 3, C5-256-Logistic-VB-40



(d) Sensor 1-3, C5-256-Logistic-VB-40

